2014

Inherent acoustic nonlinearity in fiber reinforced composites

Sunil Kishore Chakrapani
Iowa State University

Inherent acoustic nonlinearity in fiber reinforced composites

by

Sunil Kishore Chakrapani

A dissertation submitted to the graduate faculty

in partial fulfillment of the requirements for the degree of

DOCTOR OF PHILOSOPHY

Major: Engineering Mechanics

Program of Study Committee:
Vinay Dayal, Major Professor
Daniel J. Barnard
Steve Holland
Thomas Rudolphi
Wei Hong
Matthew Frank

Iowa State University

Ames, Iowa

2014

DEDICATION

I dedicate this to my family and forefathers, without whose support I would not exist in this space and time.

TABLE OF CONTENTS

ACKNOWLEDGMENTS

There are two people whom I would like to acknowledge first, my major professor Vinay Dayal and Daniel Barnard. Both of them have influenced and shaped my approach towards science from a theoretical and experimental point of view. Dr. Dayal being excellent at formulating theoretical approaches towards explaining observed phenomenon, and Dan being excellent at developing experimental procedures to confirm theoretical predictions. I am very thankful for being a part of Iowa state/CNDE for this sole reason.

I would also like to thank my committee members, Steve Holland, Thomas Rudolphi, Matt Frank and Wei Hong for their suggestions and support in putting together this work.

There are several friends whom I would like to thank for the numerous hours of FIFA and beer, which so happened to be my pressure release valve.

Finally I would like to thank my mom; Prema Chakrapani, dad; Chakrapani, and brother; Ajoy Navin Chakrapani. Their daily support helped me keep tabs on reality. Without their efforts my graduate studies would not have been possible. I would also like to thank a special someone, Jenifer Saldanha, who had to listen to hours and hours of boring idealistic philosophies and proof read my papers, surviving only by having green mint tea at stomping grounds.

ABSTRACT

Nonlinear elastic wave methods such as nonlinear resonant ultrasound spectroscopy (NRUS) and nonlinear wave modulation spectroscopy have been previously used to detect damages in several materials. It was observed that applying these techniques to composite materials becomes difficult due to the significant inherent baseline nonlinearity, i.e. nonlinearity in the undamaged state. Understanding the non-classical nonlinear nature of the composites plays a vital role in implementing nonlinear acoustic techniques for material characterization as well as qualitative nondestructive testing of composites. There are several factors which can influence the baseline nonlinear response in fiber reinforced composites, but this work is limited to the study of the effect of three factors, namely: fiber orientation, laminate sequence and type of fabric. Since fiber reinforced composites are orthotropic in nature, the baseline response variation with fiber orientation is very important. This work explores the nature of the inherent nonlinearity by performing nonlinear resonant spectroscopy (NRS) in intact or undamaged unidirectional carbon/epoxy samples with different fiber orientations with respect to major axis of the sample. Factors such as frequency shifts, modal damping ratio, and higher harmonics were analyzed to explore the non-classical nonlinear nature of these materials. Similarly, NRS tests were carried out on samples with different laminate sequence to observer the difference in nonlinear response. Similar comparisons were made between continuous fabric laminate and woven fabric laminate.

A nonlinear-viscoelastic forced vibration model based on geometric nonlinearities was developed to explain the observed responses. The Kelvin-Voigt model was used to model viscoelasticity along with geometric nonlinearity in the form of von Kármán strains. The classical nonlinear and damping sources were identified and compared between experiment and theory. A semi-analytical experimental approach was used to extract model parameters from experiment, and compare model predictions against experimental results. The classical and the non-classical nonlinear parameters were compared for different laminate sequences to complete the baseline study. Although the results presented here are for carbon/epoxy type of composites, the model and phenomenon can be extended for any fiber reinforced composite system.

CHAPTER I

INTRODUCTION

The use of composites has increased exponentially in the past decade especially in aerospace and energy sectors. With increasing demand for light weight but strong materials, composites seem to be a very effective solution. Fiber reinforced composites such as carbon fiber reinforced polymers (CFRP) and glass fiber reinforced polymers (GFRP) are extensively used in the manufacturing sector. By using these materials we make ourselves susceptible to the complexity of inspecting structures made from these materials. The field of nondestructive evaluation (NDE) has been used to catalogue various techniques for both inspection and characterization of metals. In the recent decade techniques such as ultrasonics, thermography, radiography etc. have been extended for composites in an attempt to create such a catalogue [1,2]. Ultrasonics stands out as one of the best NDE techniques for composites and has been explored by many researchers including the use of guided waves [3-8]. Typically, the damage would initiate in the form of matrix micro-cracking, matrix crushing, and fiber-matrix debonding. These defect initiators are very small and difficult to detect using traditional NDE techniques. For a tighter quality control and damage prognosis, detecting precursor to damage is very vital. Precursors such as micro-cracking or low impact delaminations are very important in determining the fatigue life of the structure. To meet this requirement several researchers have used nonlinear acoustic techniques such as nonlinear resonant ultrasound spectroscopy (NRUS) and nonlinear wave modulation spectroscopy (NWMS). These belong to a class of techniques called nonlinear elastic wave spectroscopy (NEWS) first devised by Guyer and Johnson [9]. With higher excitation amplitudes some materials begin

to act nonlinearly and deviate from linear elastic behavior even in the absence of a defect. This type of response was first reported for pristine rock and geomaterials by Guyer and Johnson [9]. They predicted that NEWS techniques can also be used for inspection of damaged materials since the characteristic response of damaged materials and geomaterials was similar. They called this class of materials as mesoscopic materials where the elastic behavior was controlled by mesoscopic elements along the grain boundary. Following this, several researchers have used NEWS techniques to detect and quantify damage in composites and other materials [10-19]. Van Den Abeele demonstrated the use of NEWS techniques for detecting damage in fiber cemented plates. The hysteresis behavior along with non-classical nonlinear indicators were summarized [10,11]. Impact damage in composite laminates and sandwich panels was investigated by Meo [14,15]. Micro-crack density from heat damage was quantified using a nonlinear parameter by Van den Abeele [16]. Aymerich [17] studied the effect of impact damage on nonlinear modulation response. It was observed that clamping force for a cantilever beam affects the nonlinear response. Novak [18] studied the evolution of nonlinear response (which was defined as read factors) for different damage states.

Layered composites constitute multiple layers of fibers, fiber-fiber overlap and fiber-matrix interface etc. This would lead one to believe that composites may exhibit mesoscopic behavior similar to rocks and concrete. The present study does not explore the possibilities of using nonlinear acoustic methods for damage detection in composites since it has been performed by various researchers [14-19]. Rather, it focuses on studying the inherent baseline nonlinearity of fiber-reinforced composites, which is the nonlinear response of the material in its intact or undamaged state. A high level of inherent

nonlinearity in the absence of a defect would make NDE of such structures very challenging. Hence understanding the baseline nonlinearity becomes very important which creates the need to characterize the baseline response and factors that may influence the baseline nonlinearity. Composites are primarily composed of binding materials (epoxy) and reinforcements (fibers). Assuming perfect bonding between fibers and epoxy and between multiple layers, the entire material can be treated as a continuum and an effective stiffness matrix can be used to describe the material. It is well known that by the same argument unidirectional laminates exhibit transversely isotropic properties, and composites in general can be described as orthotropic materials. Hence changing the fiber orientation of a unidirectional laminate would result in change in the stiffness matrix as well as the nonlinear response. To observe this phenomenon three fiber orientations were chosen, i.e. 0^0, 45^0 and 90^0, since these are standard fiber orientations chosen for making cross ply [0/90] or [45/-45], or quasi-isotropic laminate [0/45/-45/90]. Hence, the first part of the work focuses on investigating the effect of fiber orientation on the baseline nonlinearity. Many authors who have performed NRS tests on composites, both damaged and intact reported lower nonlinear response in intact state compared to damaged state. Most of these involved using quasi-isotropic or cross-ply layup. In the current study, the non-classical nonlinear (NCNL) characteristics of laminate layup for four different configurations namely [0/90], [90/0], [45/-45] and [0/45/-45/90] was also investigated. These results were compared to the results obtained from the orientation study, i.e. 0^0, 45^0 and 90^0. Furthermore, the type of fabric used for fabrication was also investigated by comparing results between continuous fabric laminate and woven laminate for [0/90] and [45/-45].

The carbon fiber/epoxy was chosen as the material system, but the results can be extended for any fiber-reinforced composite system.

1.1 Background

The nonlinear response of several materials both damaged and undamaged has been extensively explored by Johnson, Van Den Abeele, Guyer, TenCate, etc. from Los Alamos [9-12,20-23]. Van Den Abeele, Guyer and McCall [20] used a phenomenological model to show that for a nonlinear hysteretic material, linear softening (i.e. linear decrease in frequency), a quadratic dependency of the third harmonic on fundamental and linear increase of attenuation can be observed. This formulation holds good for damaged materials where the elasticity is controlled by volumetric cracks, bond systems, and other features [16]. Similar types of response was observed for rock and geomaterials by Johnson and Rasolofosaon [21] who had reported a linear decrease in frequency. Guyer et al. [22] performed a set of resonant bar experiments with geomaterials at low strains and reported a linear dependence of frequency even at very low strains ($10^{-8} \leq \varepsilon \leq 5x10^{-7}$). But in some recent research by Pasqualini et al. [23], it was reported that rocks and other geomaterials exhibit different frequency shift responses depending on the strain magnitude; (a) low strain linear zone, where the material behaves linear elastic and no frequency shift exists, (b) mid-range strain classical nonlinear zone where a quadratic decrease in frequency can be observed as shown by Landau [24], (c) high strain non-classical non-equilibrium zone where the response is controlled by slow and fast-dynamics and linear decrease in frequency can be observed. Pasqualini et al. showed that the linear softening observed experimentally in the non-equilibrium zone is due to the material conditioning effects resulting from slow dynamics. P. A. Johnson (personal correspondence) later found out

that damaged materials behave in a similar fashion and have three strain ranges as described by Pasqualini, i.e. a linear zone, a quadratic zone and a non-equilibrium zone with linear softening.

A schematic representation of each zone has been shown in Figure 1. The strain range used in the current work has also been compared to the range used by other researchers. The lowest excitation frequency as shown in the figure lies in the classical non-linear zone hence resulting in a non-zero frequency shift offset, similar to results obtained by Van den Abelee.

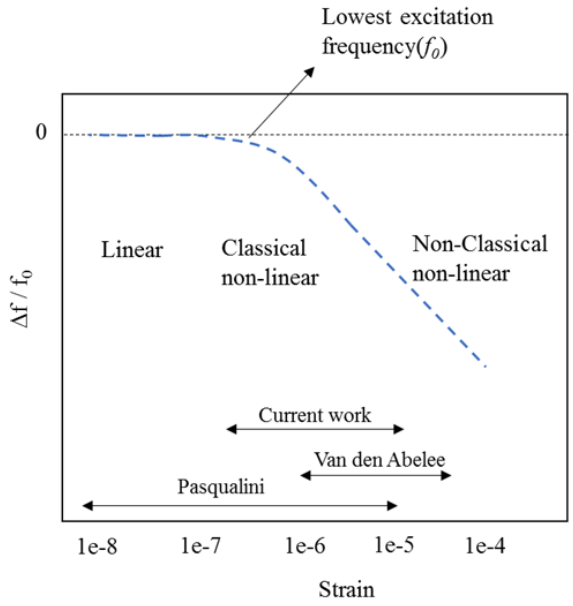

Figure 1: A schematic of the three strain zones that was observed by Pasqualini [23]. ($\Delta f/ f_0$) is the shift in the resonant frequency normalized to linear frequency. The low strain linear zone exhibits no frequency shift, while quadratic softening can be observed in the classical non-linear zone, followed by linear softening in the NCNL zone. The strain ranges used by various researchers have been compared to the strain range used in this study.

1.2 Approach

The fundamental question of whether composites belong to linear elastic, CNL or NCNL will be explored in this study. Based on the multi-material, multi-layered structure of composites, there are several factors that can influence inherent nonlinearity, such as: type of resin and fiber, fiber/matrix interface, residual stress, quality of cure, manufacturing method and ply orientation or fiber direction. We restrict this work to understanding the influence of three factors: fiber orientation, laminate sequence and fabric type on nonlinear response of fiber reinforced composites. Nonlinear resonant spectroscopy (NRS) was used to characterize the nonlinear response of different samples used in this study. Standard parameters such as resonant frequency shifts and modal damping ratio variations which have been used by several other researchers were used to comment on the baseline nonlinear response. Higher harmonic measurements were also used to analyze the nonlinear response. A forced vibration problem was framed using nonlinear von Kármán type of strains and viscoelastic damping was modeled as Kelvin-Voigt damping to arrive at a modified Duffing equation. Method of multiple scales was used to solve the modified Duffing equation. Analytically obtained results were compared against experimentally obtained results for unidirectional and multi-layered media.

CHAPTER II

EXPERIMENTAL DETAILS

2.1 Sample Preparation

A 30 layer unidirectional laminate was fabricated and 25.4 mm X 152.4 mm coupons were cut in three different orientations, namely 0^0, 45^0 and 90^0 to observe the dependency of fiber orientation on nonlinear response. The fiber direction is parallel to the length of the sample for "0^0", at 45^0 to the length for "45^0" and perpendicular to the length for "90^0". A schematic of the fiber direction and sample orientation is shown in Figure 2. Since the first order bending mode was excited during experimentation, the properties along the length of the sample will dominate the nonlinear response. Hence the fiber orientation along the length of the sample was chosen as the variable parameter. All samples were inspected by performing immersion ultrasound C-Scans and no distinct defects were found.

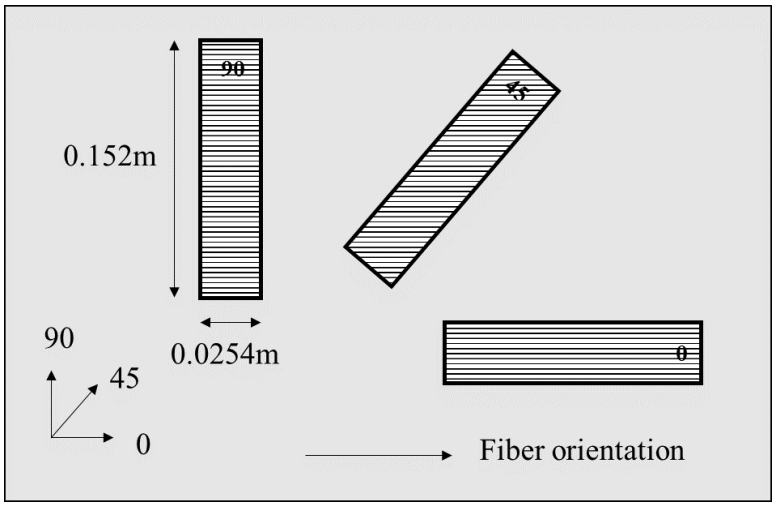

Figure 2: The schematic representation of the various samples used for experimentation are shown. Fiber direction is along the coordinate axis "0" as shown. Sample dimensions along with orientation are shown in the schematic.

2.2 Experimental Setup

A schematic of the experimental setup used is shown in Figure 3. The setup consists of a continuous waveform (CW) generator which sends a sinusoidal signal to the amplifier where the signal is amplified and sent to a magnetostrictive actuator which was used for exciting the sample. The sample was supported directly on the actuator as shown, with the head of the actuator at the geometric center of the sample. An accelerometer was used to measure the out-of-plane response of the sample and was placed at the edge of the sample. Wax was used to couple the actuator and the accelerometer to the sample. The response from the accelerometer was sent to a lock-in amplifier to track the frequency. The output from the CW generator was used as a reference for the lock-in amplifier. Data from lock-in amplifier was sent to a computer for processing.

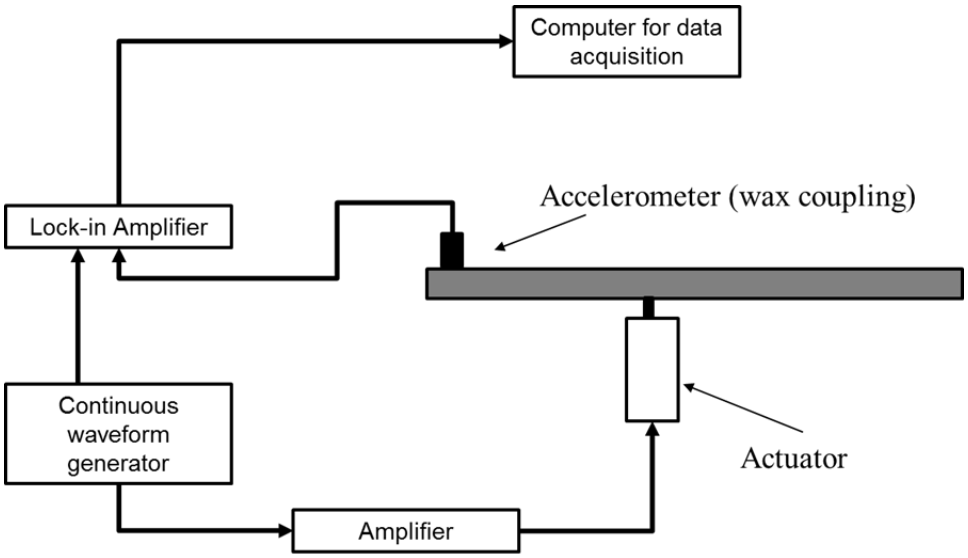

Figure 3: A schematic of the experimental setup used is shown. The sample was excited by a magnetostrictive actuator, and acceleration was recorded using an accelerometer.

2.3 Parameters Used For Characterization

Nonlinear resonant spectroscopy was performed by sweeping a broad frequency range to find the various natural modes and the lowest order mode was chosen. A 50 Hz sweep was performed on either side of the chosen resonant peak and data was collected at 16 Hz intervals. This was repeated for various levels of excitation voltages and plotted together against amplitude. Figure 4 shows the various resonance curves for 0^0.

Since "0^0" has a resonant frequency much higher than that of "90^0", the acceleration data obtained from accelerometer was converted into strain so as to normalize with resonant frequency. The laminate mounted directly on the actuator head was constrained and excited at the center.

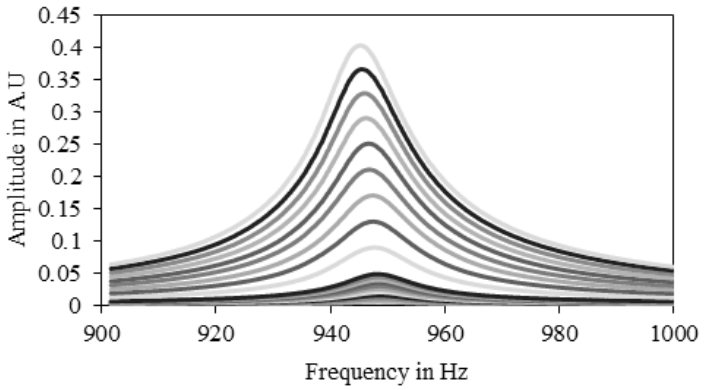

Figure 4 : Example of the resonance curves collected from the NRS test system for various levels of excitation amplitudes.

To understand the type of vibration the beam is undergoing for the given set of boundary conditions, a linear finite element modal analysis was performed. The boundary conditions chosen for the finite element analysis was that of a cantilever beam with half beam length. Modal analysis showed that the first order bending mode observed for a

cantilever beam was nominally in the same range as the experimentally observed frequency. The accelerometer position will only affect the magnitude of the measured acceleration. So in all cases accelerometer was placed at the end of the sample where maximum acceleration can be measured. Similarly the position of the actuator head will change the length of the cantilever beam resulting in a change of strain magnitude.

The strain-velocity expression used by Van Den Abeele [16,25] for free-free type of boundary condition was modified for cantilever beam with half-length as shown in Eq. (1), to match the experimental boundary conditions.

$$\varepsilon \approx 0.219 \frac{T}{f\sqrt{12}} \left(\frac{1.875}{L/2}\right)^2 v \tag{1}$$

where v is the velocity determined by integrating the acceleration data over time, L = 152.4 mm and T = 4 mm are the sample dimensions, and f is the resonant frequency. Further to determine attenuation or modal damping ratio (MDR) [10], the MDR formula was used as shown in Eq. (2).

$$MDR = {Q^{-1}}/{2} = {\frac{f_{hw}}{f}}/{2} \tag{2}$$

where f_{hw} is the frequency width at half the peak amplitude of the resonant peak (f) at finite strain amplitude. MDR has been used by many researchers to show non-classical nonlinear responses [10]. In the linear zone, MDR remains a constant and does not change. At higher strains, a linear increase in MDR can be observed for NCNL materials.

CHAPTER III

INFLUENCE OF FIBER ORIENTATION

3.1. Frequency Shift

NRS test was repeated for all three orientations and resonance curves at increasing levels of excitation was collected. Figure 5 shows the resonance curves for three orientations. A varying degree of shift in frequency can be observed.

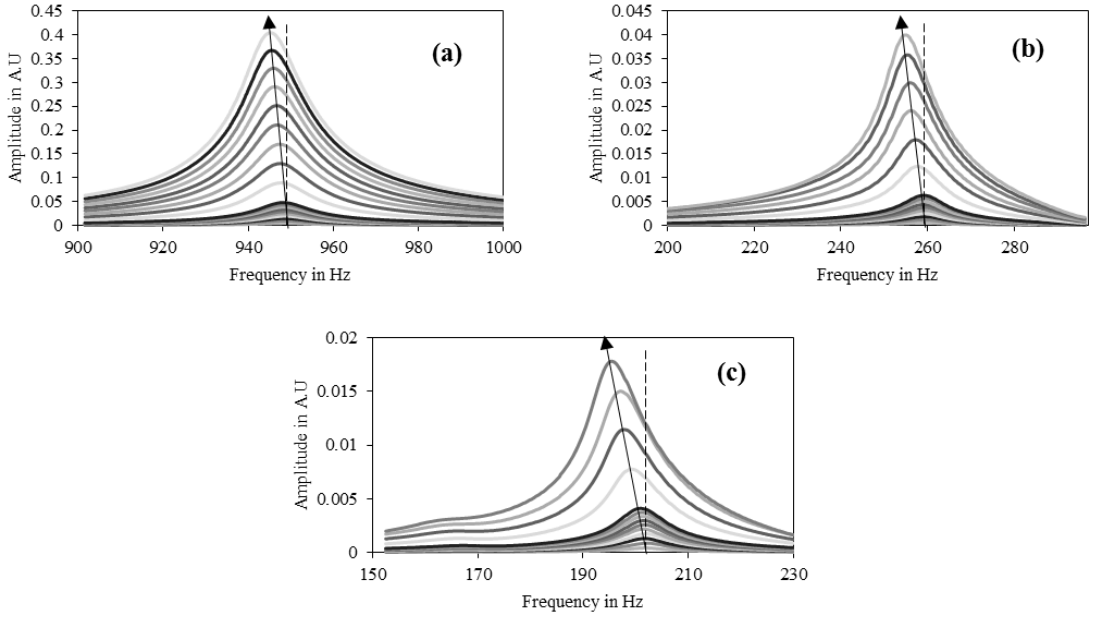

Figure 5: Resonance curves for various levels of excitation amplitudes. (a) 0^0, (b) 45^0 and (c) 90^0 laminate.

Shift in resonance frequency was calculated by: $\Delta f = f - f_0$, where f_0 is the lowest amplitude excitation frequency. Since the lowest excitation frequency is different for different orientations, the frequency shift was normalized to the resonant frequency at lowest excitation ($\Delta f / f_0$). The frequency shifts for 0^0, 45^0 and 90^0 are presented in Figure 6. Maximum shift was observed for 90^0, followed by 45^0 and 0^0. All strain data was limited

to 15 micro-strain. A nominally linear frequency shift was observed with increasing strain amplitude over the data range. This overall response is consistent with non-classical non-linear materials. Although a good linear fit over the entire strain can be observed, fits over smaller ranges has to be performed to observe changes in nonlinear behavior.

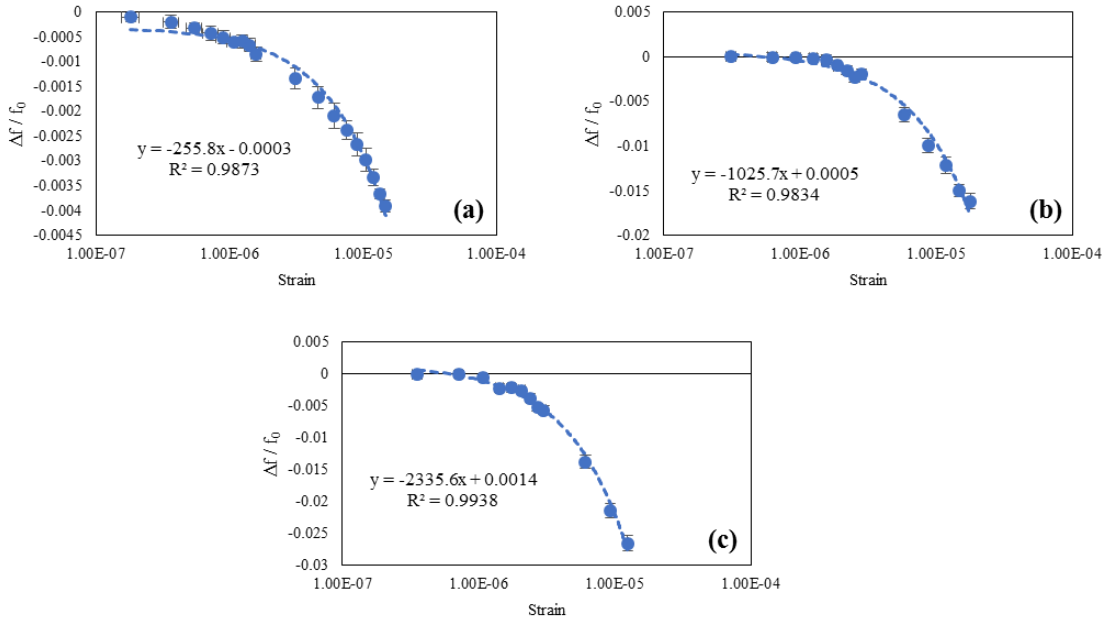

Figure 6: Shift in resonant frequency normalized to low amplitude frequency for different orientations. (a) 0^0, (b) 45^0 and (c) 90^0. Note the logarithmic scale for strain. The error bars have also been plotted in the data along with R^2 values and equations for linear fit.

The presence of a quadratic softening zone was investigated by performing a pure quadratic fit on the experimental data starting from low strain to the high strain amplitude. A comparison between quadratic fit and linear fit over the low range for 45^0 laminate can be seen in Figure 7. The R^2 value for linear fit over the small range was 0.801 compared to 0.9834 for the linear fit over the entire range. This shows that a discontinuity exists, which is an indicator that the material does not exhibit linear softening over the entire range. The R^2 value for a pure quadratic fit (0.89) was better than the R^2 value for the linear fit (0.801)

which suggest the presence of the quadratic softening zone or the classic nonlinear zone. Information in the CNL zone can be affected by various experimental factors such as humidity, temperature etc. Furthermore because of a gradual transition from the CNL to NCNL zone, results will necessarily be influenced by both responses.

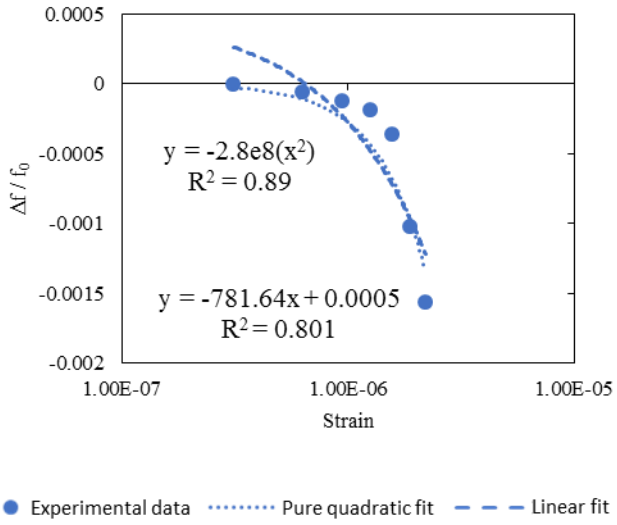

Figure 7: The frequency shift in lower strain range for 45^0 sample. A pure quadratic fit and linear fits were compared using their respective R^2 values. From the R^2 values the quadratic fit seems to be better than the linear fit in this range. The R^2 value for the linear fit over the entire range as shown in Fig. 6(b) is 0.983, but linear fit over the low strain range is 0.801, which shows the discontinuity in response.

The pure quadratic fits in the small range were extrapolated for the entire range and plotted against the experimental data as shown in Figure 8. A good quadratic fit can be observed for a certain strain range beyond which the experimentally observed data deviates from the quadratic fit. Comparing the goodness of fit in the low strain range as 45^0, the quadratic fit R^2 value for 0^0 was 0.61 compared to linear fit value of 0.969. This can be due to the gradual transition between CNL and NCNL zone as suggested earlier. Further to get a good quadratic fit, data in the linear strain range and CNL range has to be measured as

shown by Pasqualini. Since the data for 0^0 starts in the CNL range and transitions quickly to NCNL range within a short strain range, the R^2 value for quadratic fit will be lower than the linear fit. However there are sufficient points in the NCNL range for 0^0 to describe a good linear fit confirming the NCNL response. The quadratic fit R^2 value for 90^0 was 0.965 compared to linear R^2 value of 0.945 which is consistent with 45^0. To be able to truly characterize the linear, CNL and NCNL strain zones, a measurement similar to Pasqualini has to be performed over a large strain range under controlled environment. This is considered out of scope of this study since the objective is to characterize the NCNL zone of these materials. Linear softening with increasing strain amplitude indicates NCNL behavior. Further, the presence of two zones, namely quadratic softening zone and non-equilibrium zone with linear softening at higher strains suggests that these materials can be classified under NCNL type of materials.

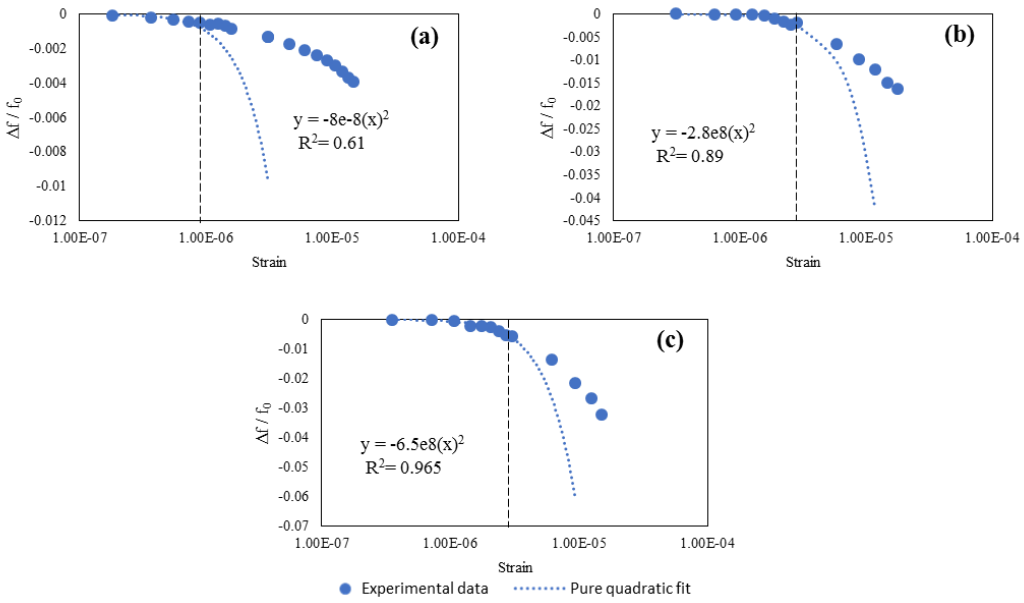

Figure 8: Frequency shift vs strain showing the two zones, namely: classical nonlinear and non-classical nonlinear. A pure quadratic fit is compared with experimental data to show the threshold strain where the material begins to lose its quadratic nature and behave like a NCNL material.

3.2 Modal Damping Ratio

Since 0^0, 45^0 and 90^0 have different MDR values, relative change in MDR was used as shown in Eq. (3).

$$\Delta MDR = \frac{Q^{-1} - Q_0^{-1}}{2} \tag{3}$$

where, $Q^{-1}/2$ is the MDR at higher strain amplitude, and $Q_0^{-1}/2$ is the MDR at the lowest excitation amplitude. The MDR calculated from Eq. (3) was plotted for all three samples against strain as shown in Figure 9. A linear increase in MDR was observed for all samples with 90^0 exhibiting the maximum increase, followed by 45^0 and 0^0. The linear increase in MDR suggests NCNL characteristics. The dependency of MDR on the fiber orientation is consistent with results obtained from frequency shifts.

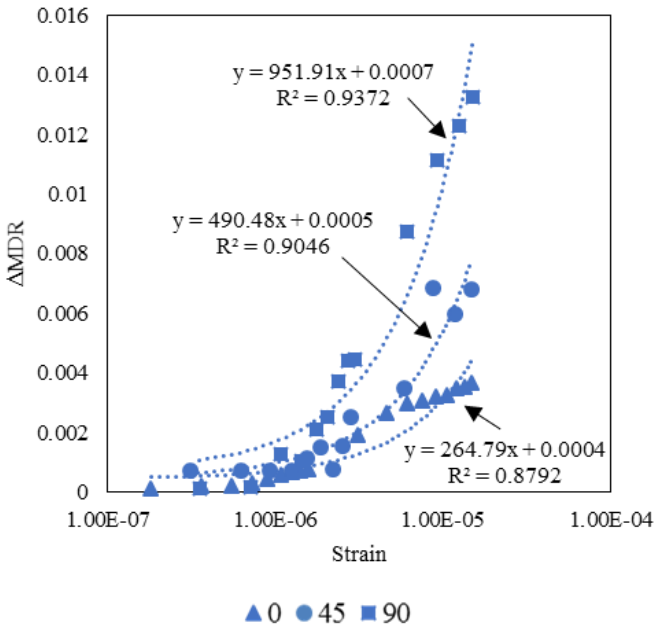

Figure 9: Modal damping ratio increase for different orientations showing a linear fit. Highest increase in MDR with increasing strain can be observed for 90^0 followed by 45^0 and 0^0, which is consistent with the frequency shift response. Note the logarithmic scale for strain.

3.3 Higher Harmonic Analysis

To further explore the presence of non-classical behavior, a higher harmonic analysis was performed on each sample. Frequency sweeps were performed to find the fundamental resonant frequency, and the amplitude of higher harmonics were measured for the given excitation voltage. The process was repeated for different excitation voltages. To explore the NCNL aspect, a pure cubic fit was performed on the 3^{rd} harmonic experimental data for all three orientations as shown in Figure 10. A pure quadratic fit was also performed on the experimental data to compare with cubic fit. Fitting was performed from the low strain range to the high strain range due to the discontinuous nonlinear response as shown earlier in frequency shifts. R^2 values were used to compare the goodness of fit between the quadratic and cubic fits. From Figure 10, it is evident that the 3^{rd} harmonic does not follow a cubic dependency of the fundamental which suggests the absence of CNL characteristics. A pure quadratic fit seems to match the experimental data well for both 0^0 and 45^0. The quadratic R^2 value for 0^0 was 0.989 compared to the cubic fit which was 0.66 which shows that a quadratic fit is better. Similarly the quadratic R^2 value for 45^0 was 0.9931 compared to 0.4771 for the cubic fit which shows a better quadratic fit. However for 90^0, the experimental response lies somewhere between a quadratic and cubic response since the quadratic R^2 value is 0.861 compared to the cubic response of 0.964. This suggests contributions from both CNL and NCNL for the given excitation range. Although the third harmonic response for 90^0 is somewhat ambiguous, the increase in MDR and frequency shift of the sample are indicative of NCNL response. By fitting the data from low strain to high strain amplitude, it can observed that beyond a particular acceleration (strain) the 3^{rd} harmonic loses its classic nonlinear response (cubic

dependency) and begins to exhibit non-classical nonlinear response (quadratic dependency). The 3rd harmonic scaling quadratic with the fundamental suggests NCNL characteristics.

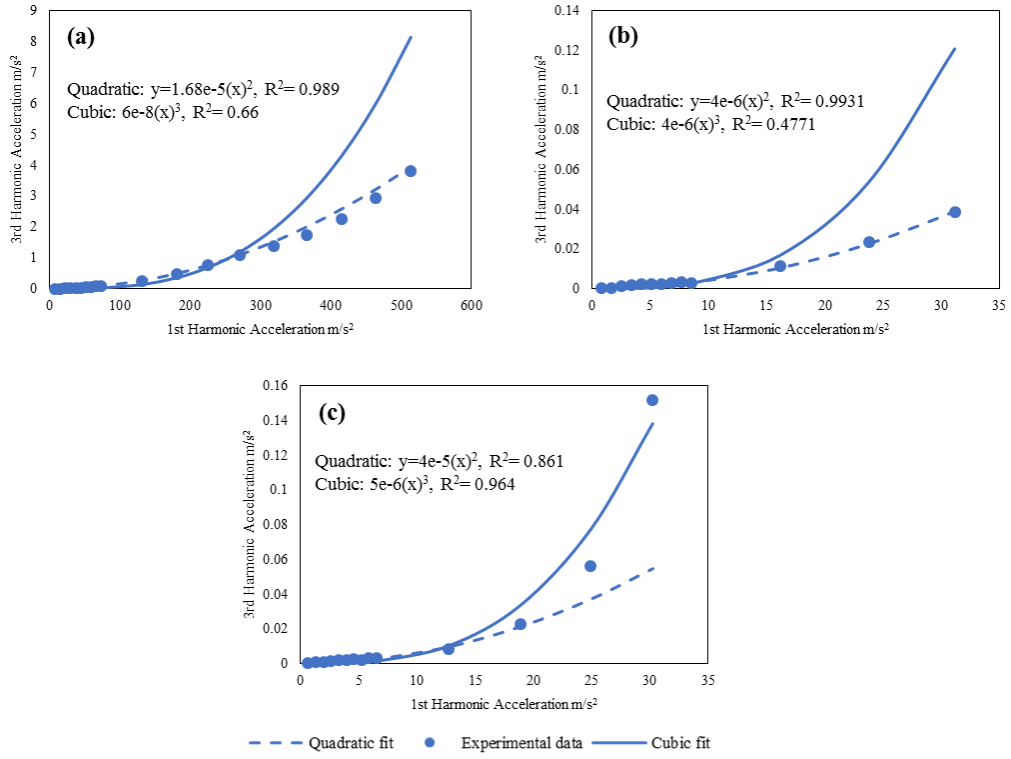

Figure 10: 3rd harmonic acceleration values have been plotted against fundamental acceleration values for (a) 0^0, (b) 45^0 and (c) 90^0. In each case a pure quadratic and cubic fit was also performed to investigate quadratic or cubic dependency. The difference in the scale of fundamental acceleration for 0^0 compared to 45^0 and 90^0 arises from different fundamental frequencies. The R^2 values for cubic and quadratic fits have also been listed.

From the results presented in this chapter it can be observed that composites exhibit NCNL characteristics. The frequency shift, MDR and harmonic analysis results are consistent and shows that unidirectional fiber reinforced composites exhibit NCNL properties. It can also be noticed from Figure 7 and 8 that there exists a CNL zone where quadratic softening can be observed. This is consistent with results presented by Pasqualini et al. [23].

CHAPTER IV

EFFECT OF LAMINATE SEQUENCE

This section presents the effect of laminate sequence on the nonlinear response of composites. A laminate with $[0]_{15s}$ corresponds to symmetric, 0^0,15 layer laminate (total 30 layers). By changing the orientation of the individual layers, the laminate essentially becomes a multi-layered media, and the properties of laminate can be tailored. A [0/90] 30 layer symmetric laminate was fabricated and 25.4 mm X 152.4 mm coupons were cut in three different orientations. The global axis for the [0/90] laminate is shown in Figure 11. Since NRS utilized the flexural mode, the properties along the length of the laminate will influence the nonlinear response. As shown in Figure 11, the coupons were cut at 0^0, 45^0 and 90^0 to the global axis. The sample at 0^0 to the global coordinate is [0/90], the sample at 45^0 is [45/-45] and sample at 90^0 is [90/0]. A 48 layered quasi-isotropic (QIS) laminate with [0/45/-45/90]6s was also fabricated.

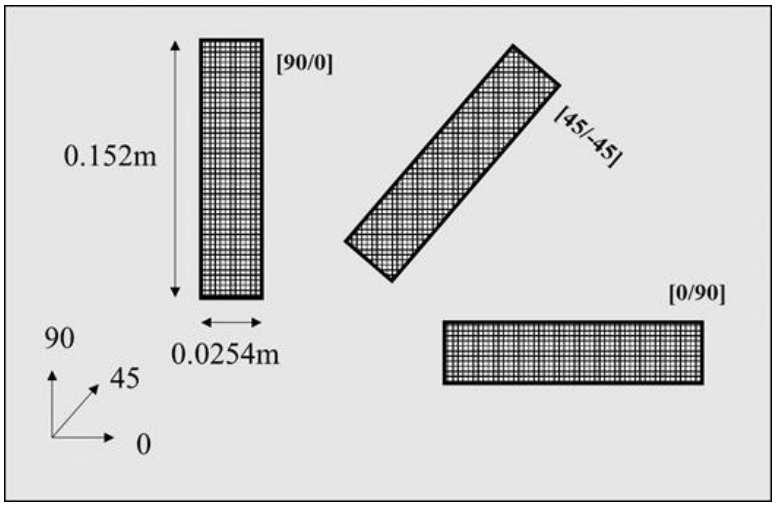

Figure 11: The schematic representation of the various samples used for experimentation are shown. Fiber direction is along the coordinate axis "0" and "90". The various laminate sequences resulting from cutting the samples are different orientations are listed next to the samples. Sample dimensions along with orientation are shown in the schematic.

All samples used in this study were symmetric laminates. They were scanned, inspected with immersion C-Scans and no distinct defects were found.

NRS tests were carried out on the [0/90], [90/0], [45/-45] and [0/45/-45/90] samples. Figure 12 shows the normalized frequency shift vs. strain amplitude plot for the different laminate sequences. It is evident from Figure 12(a) and 12(b) that although [0/90] and [90/0] are different only by 2 plies, a difference in nonlinear properties can be observed. Since [90/0] has more number of 90^0 plies, its NCNL characteristic is slightly higher than that of the [0/90]. The [45/-45] has a much bigger shift compared to [0/90] sequence. The quasi-isotropic sequence, [0/45/-45/90] seems to exhibits a much smaller frequency shift compared to the cross ply sequence.

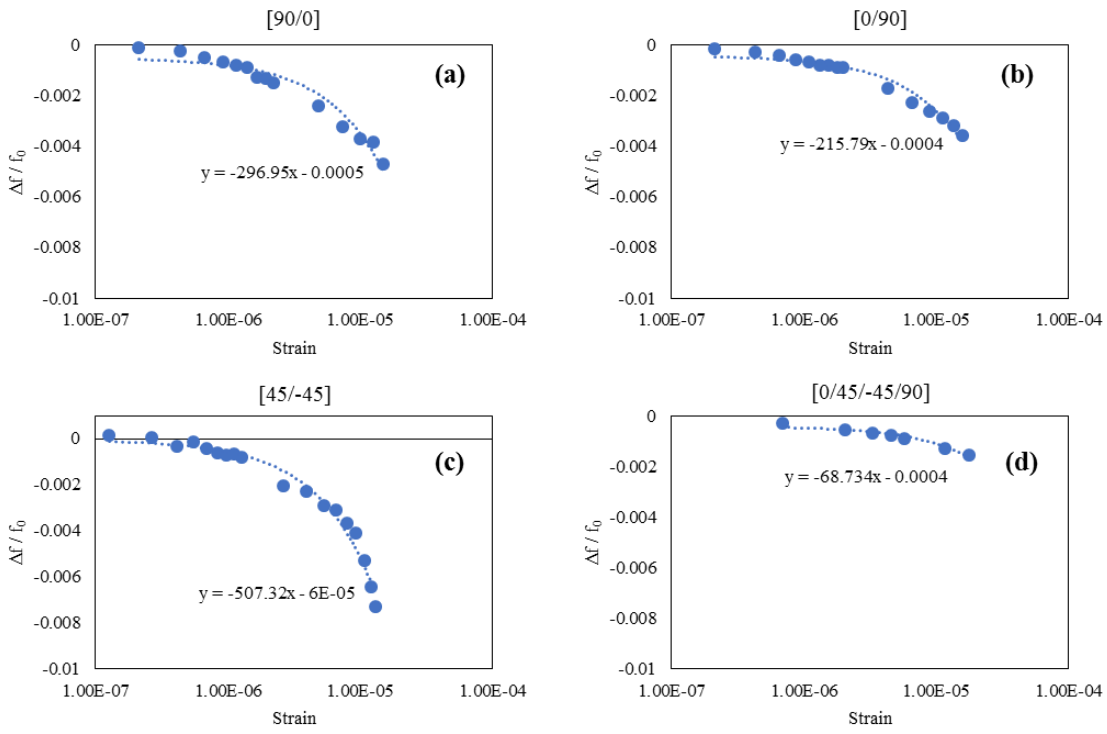

Figure 12: Frequency shifts of different laminate sequences are compared: (a) [90/0], (b) [0/90], (c) [45/-45], (d) [0/45/-45/90]. Note the log scale used to plot the strain.

To get a perspective of how the nonlinear shifts for multi-layered media (MLM) look compared to unidirectional (UD) laminates, i.e. 0^0, 45^0 and 90^0, the frequency shifts of the MLM were plotted together with the UD as shown in Figure 13. It can be observed that MLM NCNL response is less than or almost the same as the 0^0 laminate response. The lowered NCNL response of MLM compared to UD suggests that as anisotropy of the laminate decreases, the NCNL response also decreases (the quasi-isotropic laminate is closer to isotropic than the transversely isotropic nature of UD).

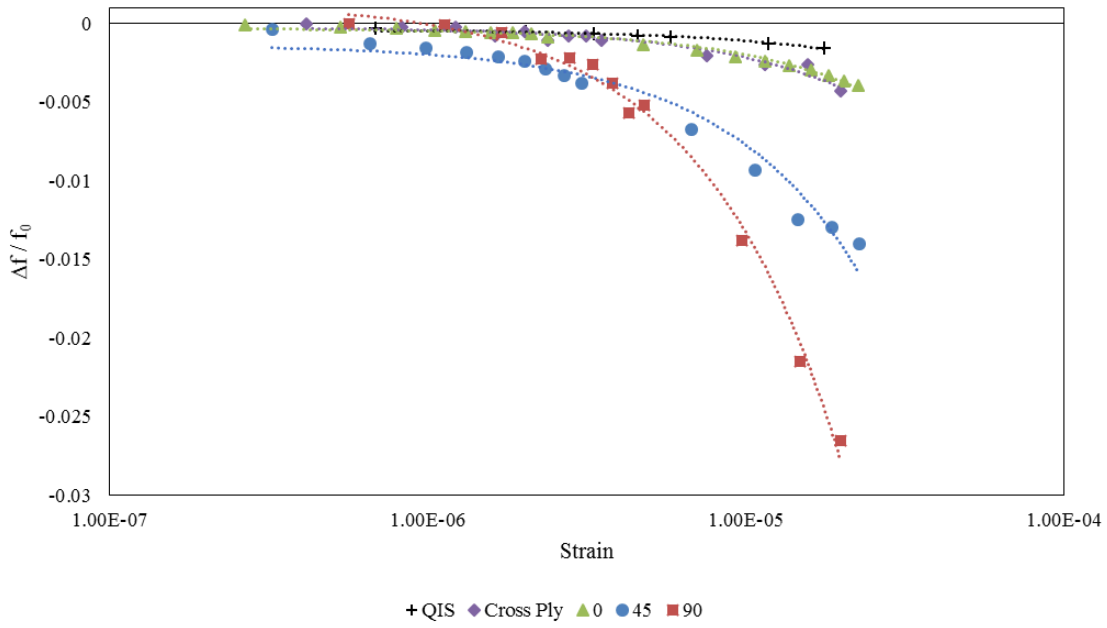

Figure 13: The frequency shifts observed for MLM have been compared with UD laminate. Cross ply signifies [0/90] in this plot. The frequency shifts for MLM are much lower compared to the UD laminates. Note the log scale used to plot the strain.

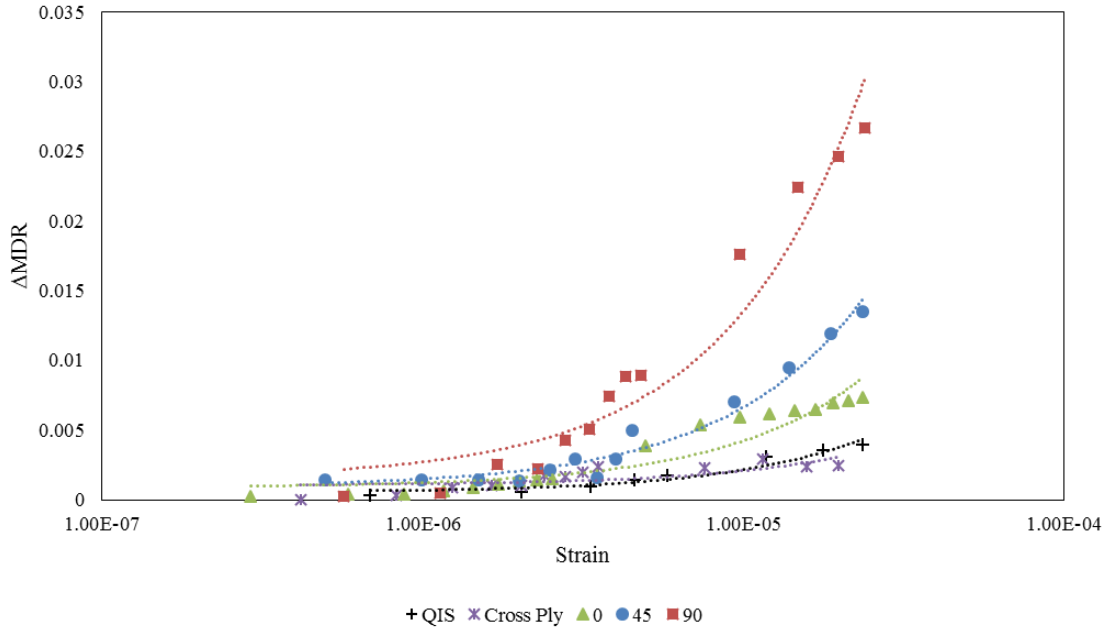

Figure 14: The MDR shifts observed for MLM have been compared with UD laminate. MDR shifts for MLM are much lower compared to the UD laminates and trends are consistent with the frequency shifts observed in Fig. 15. Note the log scale used to plot the strain.

The MDR shift vs. strain was plotted as shown in Figure 14. Similar to the frequency shift results, the MDR shift of MLM was considerably lower than the UD laminates. The quasi-isotropic and cross ply laminates exhibits least increase in MDR, lower than the 0^0 laminate. The MDR shift results are consistent with the frequency shift results, i.e. MLM has a much lower MDR shift compared to the UD.

Although the reason behind this behavior is not directly apparent, it can be concluded that laminate sequences which make the laminate closer to being isotropic, decreases the NCNL characteristics of the laminate.

CHAPTER V

EFFECT OF FABRIC TYPE

There are two types of fabrics which are used in composite fabrication; continuous fabrics, where individual fiber and fiber toes are aligned in one direction which forms a continuous strand and woven fabrics, where the fiber bundles are woven in a particular pattern so that the strands interlace with other strands at right angle. Examples of the commonly used weave pattern are plain, twill and satin weave, which include 4, 5 and 8 harness weaving pattern. Due to the weaving and interlacing, it can be hypothesized that fiber-fiber interaction might be higher in this type of laminate compared to continuous fabric laminates, which might give rise to a higher NCNL response. A 4 harness satin weave sample of nominally the same thickness as that of the [0/90] continuous laminate was fabricated. Two 25.4 mm X 152.4 mm coupons were cut from the laminate at 0^0 and 45^0 similar to the samples described in Chapter IV. From here on the 0^0 laminate will be called as woven cross ply (WCP) and the 45^0 laminate will be called as [45/-45]W.

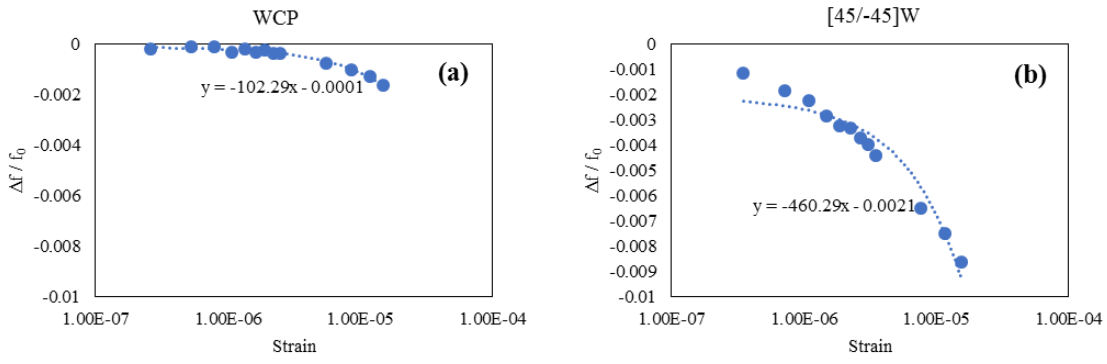

Figure 15: The observed frequency shifts from woven fabric laminates; (a) WCP, (b) [45/-45]W. WCP stands for woven cross ply and is the equivalent of [0/90] for continuous fabric.

NRS tests were carried out on WCP and [45/-45]W laminates. The frequency shift response can be seen in Figure 15(a) & (b). It can be observed that [45/-45]W has a much higher NCNL response compared to the WCP, similar to the continuous fabric results. To get a perspective of how different the NCNL response is between woven and continuous fabric, the frequency response was plotted together as shown in Figure 16. It can be observed from Figure 16(a) & (b) that WCP exhibits lower NCNL response compared to both [0/90] and [90/0]. But, [45/-45]W exhibits a slightly higher nonlinear response in the classic zone compared to [45/-45]C, whereas the NCNL response of [45/-45]C is slightly higher than [45/-45]W as can be seen from the slope of the linear fit.

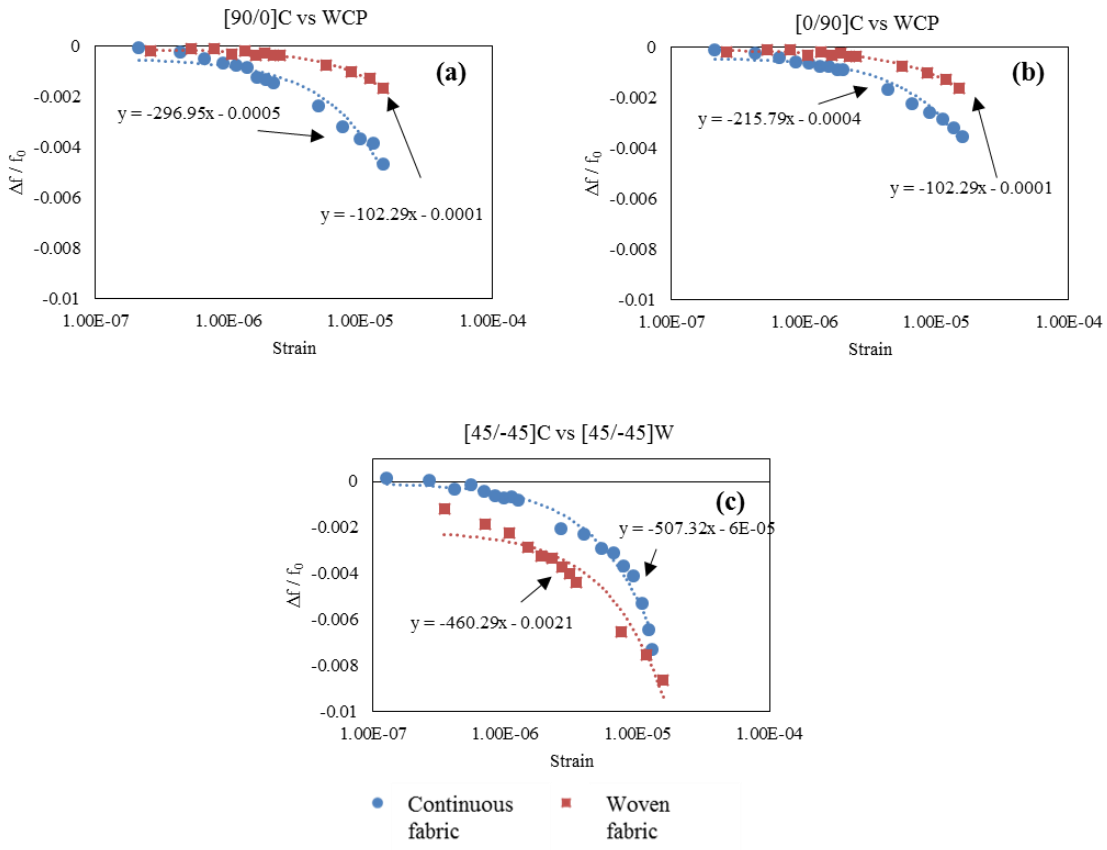

Figure 16: Frequency shifts for woven and continuous fabric compared between: (a) [90/0]C vs. WCP, (b) [0/90]C vs. WCP, (c) [45/-45]C vs. [45/-45]W. The woven fabric exhibits lower nonlinearity compared to the continuous fabric.

To confirm the findings a higher harmonic analysis was carried out. The 2nd and 3rd harmonic of resonant frequency for continuous and woven laminates were measured for increasing excitation voltages. The measured harmonic accelerations were plotted against the fundamental acceleration. Figure 17 shows various plots comparing the continuous and woven fabric. Figure 17(a) & (c) show that the 2nd harmonic amplitude for [0/90] and [90/0] compared to WCP are nominally similar for the considered acceleration range. Fig. 17(e) also shows a similar trend with the woven laminate having a slightly lower 2nd harmonic content than the continuous laminate. Figure 17(b), (d) and (f) tell a completely different story, i.e. the continuous fabric exhibits much higher 3rd harmonic content than the woven laminate. One of the attributes of NCNL materials is that they exhibit a higher 3rd harmonic content compared to classic nonlinear materials. The higher NCNL response from continuous fabric compared to woven fabric confirms the frequency shift results.

Contrary to the earlier hypothesis that woven fabric might exhibit higher NCNL response than continuous fabric, results show that woven fabrics exhibit lower NCNL characteristics than continuous fabric laminates. It is difficult to provide a theoretical explanation for the lower nonlinearity exhibited by woven laminates. One of the possible reasons might be that the interlacing of the fabric tends to inhibit any shear/ sliding action of the fabric. This shear/sliding action is one of the main contributors of the non-classical effects. Similarly any type of inter-lamina shearing is also inhibited in woven laminate, whereas it exists in continuous laminate. A much deeper understanding of the non-classical nonlinear phenomenon is required to build a theory around the experimental observations.

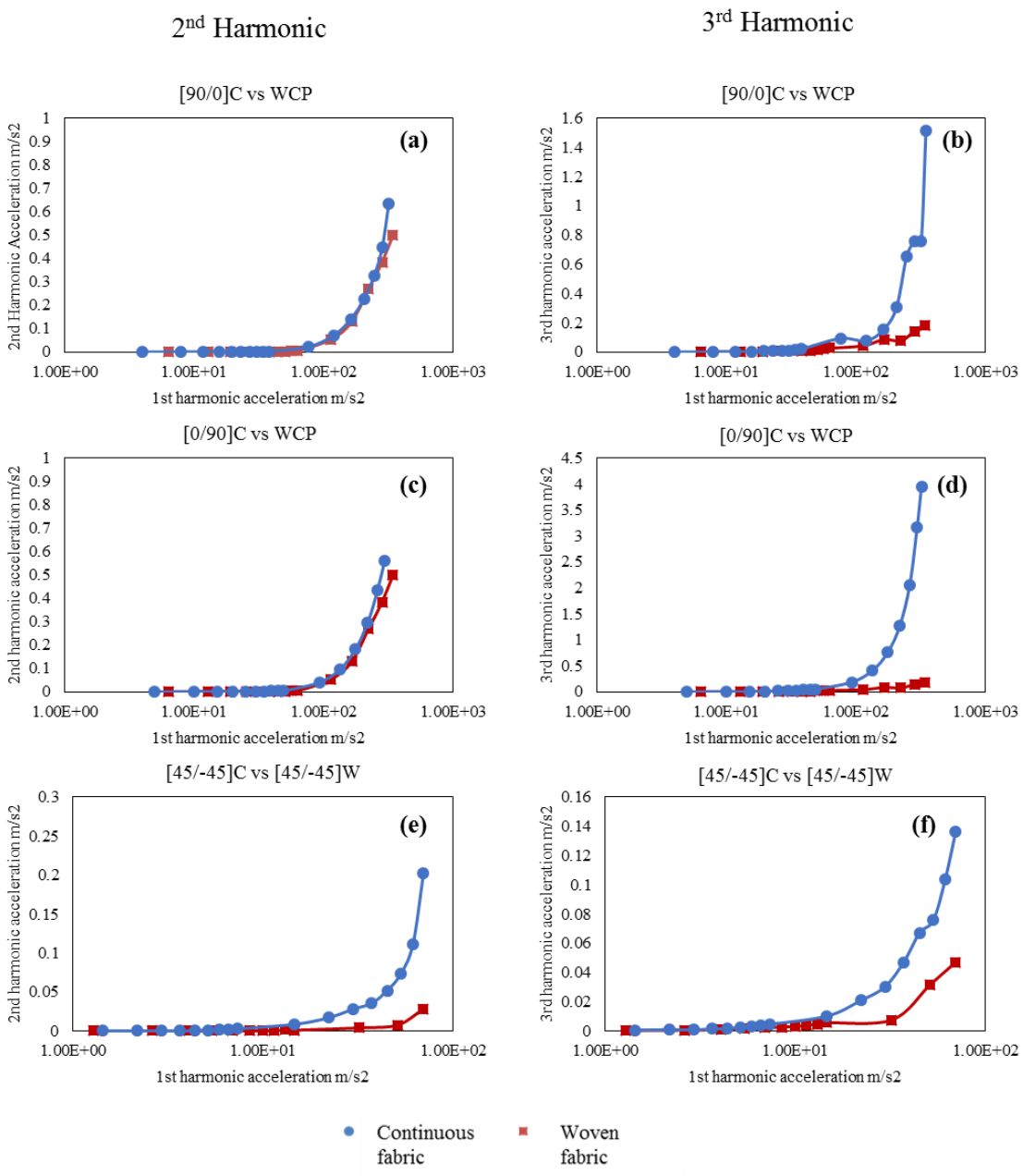

Figure 17: The higher harmonic content measured for continuous fabric has been compared with the woven fabric. Figures (a), (c) and (e) represent the 2nd harmonic acceleration plotted against the fundamental acceleration. Figures (b), (d) and (f) represent the 3rd harmonic acceleration plotted against the fundamental acceleration. Comparisons between WCP and [0/90]C and [90/0] in (a) and (c) show that the 2nd harmonic contents are quite similar, while the 3rd harmonic content is much higher in the continuous fabric (b) and (d). Similar results can be observed between [45/-45]C and [45/-45]W. The line connecting the dots are only for presentation and do not represent a fit.

CHAPTER VI

NONLINEAR FORCED VIBRATION MODEL

From the experimental observations in the previous chapters it is evident that the epoxy or matrix plays a vital role in the non-classical nonlinear response. The [90] laminate exhibited higher levels of nonlinearity compared to [0]. It is well known that the properties of [90] are influenced by matrix rather than the fibers. Similarly, it can be observed from laminate sequence results that as the laminate gets closer to being isotropic in nature, the non-classical nonlinearity reduces. A quasi-isotropic laminate will have fibers in multiple directions, which reduces the influence of matrix. Hence to explain the observed phenomenon, a nonlinear forced vibration model was developed. Building such a model will also allow characterization of the baseline nonlinearity observed in laminates with different fiber orientations and stacking sequences without the need to fabricate and test them. Moreover such a model could also be applied for any fiber reinforced system, not just carbon/epoxy.

Several researchers have built forced vibration models for both nonlinear and linear analysis. The use of analytical formulation, or finite element or combination of both having a semi-analytical finite element formulation is very common. A semi-analytical approach was used for examining the forced and free vibration of S-S and C-C beams by Azrar et al [26,27]. Mahmoodi et al. [28,29] who investigated the nonlinear vibration of a cantilever viscoelastic beam by modeling it as an Euler-Bernoulli beam with Kelvin-Voigt damping. A two layered model with carbon nanotube-epoxy mixture was studied both analytically and experimentally. Youzera et al. [30] studied a three layer beam with composite core using a nonlinear damped model by performing forced vibration analysis. Shooshtari et al.

[31] studied nonlinear forced vibration of clamped functionally graded beams without damping.

It is well know that composites constitute two materials, the fiber and epoxy which have completely different properties. Hence, there are several factors which have to be included in a unified model to capture all the effect, such as fiber-matrix interface, shear/sliding effects from fiber-fiber interaction, and inter-lamina effects. But a grand unified model including all these factors is not possible with the current understanding of the scale and effects of such factors. Hence, in the current study a continuum approach towards modeling was used. A comparison between analytical and experimental nonlinearity parameters will also help to identify the difference that arises by neglecting or discounting these factors.

It can be observed from experiments that the coupon can be treated as cantilever beam undergoing flexural vibrations. Since the coupon is composite with orthotropic properties, the beam can be modeled as a laminated beam. Using an approach similar to other researchers [28, 31] a nonlinear forced vibration analysis can be developed using geometric nonlinearity. The current study extends this to include the effect of viscoelasticity by using the Kelvin-Voigt model for stress-strain relationship. This viscoelastic contribution comes from the matrix, and by modeling a laminated beam, the effect of fiber orientation and stacking sequences can be captured.

The present model follows the *classical laminated plate theory* (CLPT) [32]. According to Kirchhoff hypothesis, the displacements are given as:

$$u(x, y, z, t) = u_0(x, y, t) - z\frac{\partial w_0}{\partial x} \tag{4}$$

$$w(x, y, z, t) = w_0(x, y, t) \tag{5}$$

Where t is the time and u_0 and w_0 are the in-plane and transverse mid-plane displacements. The von Kármán type nonlinear strain-displacement relationship is given by:

$$\varepsilon_{xx} = \frac{\partial u_0}{\partial x} + \frac{1}{2}\left(\frac{\partial w_0}{\partial x}\right)^2 - z\frac{\partial^2 w_0}{\partial x^2} \tag{6}$$

Assuming the solid to be viscoelastic, a linear elastic stress-strain relationship together with Kelvin-Voigt damping term for the viscoelastic contribution is given by:

$$\sigma = E\varepsilon + \eta\dot{\varepsilon} \tag{7}$$

where, E is the Young's modulus which can be written as stiffness matrix, η is the Kelvin-Voigt damping term which controls the strain rate. Eq. (7) can be written as:

$$\sigma = \sigma_e + \sigma_v \tag{8}$$

where, σ_e is the elastic component of the stress-strain response, and σ_v is the viscoelastic component.

By using the extended Hamilton's principle;

$$\delta \int_0^T (K - \Pi + W)\, dt = 0 \tag{9}$$

where, K is the kinetic energy, Π is the potential energy, and W is the work done by non-conservative forces. Potential energy can be rewritten as: $\Pi = U + V$, where U is the elastic strain energy and V is potential energy change from conservative external forces.

Writing out in virtual terms separately:

$$\delta U = \oiint_{-h/2}^{h/2} (\sigma_e \delta\varepsilon_{xx}) dz\, dxdy \tag{10}$$

$$\delta V = -\oiint_{-h/2}^{h/2} \Big(\big(F\delta w(x, y)\big)\Big) dzdxdy \tag{11}$$

$$\delta K = \oiint_{-h/2}^{h/2} \left(\rho_0 \left[\left(\dot{u}_0 - z\frac{\partial \dot{w}_0}{\partial x}\right) + \left(\delta\dot{u}_0 - z\frac{\partial \delta\dot{w}_0}{\partial x}\right) + \dot{w}_0\delta\dot{w}_0\right]\right) dzdxdy \tag{12}$$

$$\delta W = -\oiint_{-h/2}^{h/2} (\sigma_v \delta\varepsilon_{xx}) dz\, dxdy \tag{13}$$

where F is the external force applied, σ_v is the non-conservative viscous dissipative force, and the $\delta\varepsilon_{xx}$ and δu_0, δw_0 are the virtual strain and virtual displacements.

Substituting Eq. (10-13) into (9) we obtain:

$$\int_0^T \left(\oiint_{-h/2}^{h/2} \left((\sigma_e + \sigma_v)\delta\varepsilon_{xx} - (F\delta w_0) \right.\right.$$

$$\left.\left. - \rho_0 \left[\left(\dot{u}_0 - z\frac{\partial \dot{w}_0}{\partial x}\right) + \left(\delta\dot{u}_0 - z\frac{\partial \delta\dot{w}_0}{\partial x}\right) + \dot{w}_0\delta\dot{w}_0\right]\right) dzdxdy \right) dt = 0 \tag{14}$$

Using Eq. (8), the elastic and viscous stress can be rewritten and Eq. (14) can be solved to obtain the equations of motion:

$$\frac{\partial N_{xx}}{\partial x} = I_0 \frac{\partial^2 u_0}{\partial t^2} \tag{15}$$

$$\frac{\partial}{\partial x}\left(N_{xx}\frac{\partial w_0}{\partial x}\right) + \frac{\partial^2 M_{xx}}{\partial x^2} + F = I_0 \frac{\partial^2 w_0}{\partial t^2} \tag{16}$$

where N_{xx} and M_{xx} are the force and moment resultants and I_0 is the mass moment of inertia given by:

$$N_{xx} = \int_{-h/2}^{h/2} \sigma_{xx} dz \tag{17}$$

$$M_{xx} = \int_{-h/2}^{h/2} \sigma_{xx}(z) dz \tag{18}$$

$$I_0 = \int_{-h/2}^{h/2} (\rho_0) dz \tag{19}$$

Rewriting the nonlinear strain relationship:

$$\varepsilon_{xx} = u_0' + \frac{1}{2}(w_0')^2 - w_0'' \tag{20}$$

Where, the term u_o' corresponds to partial differential with respect to *x*.

Substituting Eq. (20) and (7) into (17) and (18) gives:

$$N_{xx} = A_{11}\left(u_0' + \frac{1}{2}(w_0')^2\right) - B_{11}w_0'' + \mu(\dot{u}_0' + w_0'\dot{w}_0'') - \mu'\dot{w}_0'' \tag{21}$$

$$M_{xx} = B_{11}\left(u_0' + \frac{1}{2}(w_0')^2\right) - D_{11}w_0'' + \mu'(\dot{u}_0' + w_0'\dot{w}_0'') - \mu''\dot{w}_0'' \tag{22}$$

where,

$$(A_{11}, B_{11}, D_{11}) = \int_{-h/2}^{h/2} C_{11}(1, z, z^2)dz \tag{23}$$

$$(\mu, \mu', \mu'') = \int_{-h/2}^{h/2} \eta(1, z, z^2)dz \tag{24}$$

For symmetric laminates the bending-extensional coupling parameter B_{11} and μ' are negligible. By neglecting axial inertia, the in-plane force resultant (N_{xx}) becomes invariant of *x*, i.e. $(dN_{xx}/dx) = 0$. The in-plane displacements become small allowing us to write the force and moment resultants in terms of the transverse displacement. Assuming the force resultants don't change over time, integrating over time and length, the new force and moment resultants are obtained as:

$$N_{xx} = \int_0^T \int_0^L \left[A_{11}\left(\frac{1}{2}(w_0')^2\right) + \mu(w_0'\dot{w}_0'')\right] dxdt \tag{25}$$

$$M_{xx} = -D_{11}w_0'' - \mu''\dot{w}_0'' \tag{26}$$

For nonlinear vibration analysis, expressing the transvers displacement as:

$$w(x,t) = q(t)\, p(x) \tag{27}$$

where, *q(t)* corresponding to temporal function and *p(x)* corresponds to spatial function or linear vibration mode shape. Substituting Eq. (27) into force and moment resultant equations, Eq. (25), (26) and re-substituting those into the equation of motion, Eq. (16), we can obtain the nonlinear equation:

$$\ddot{q} + (\beta^2)q + (\gamma)q^3 + (\delta)q^2\dot{q} + (\alpha)\dot{q} = F \tag{28}$$

where,

$$\beta^2 = \frac{D_{11}}{\Delta}\int_0^L p^{IV}dx \tag{29}$$

$$\gamma = -\frac{A_{11}}{2\Delta}\int_0^L p''dx \int_0^L (p')^2 dx \tag{30}$$

$$\delta = -\frac{\mu}{2\Delta}\int_0^L p''dx \int_0^L (p')^2 dx \tag{31}$$

$$\alpha = \frac{\mu''}{\Delta}\int_0^L p^{IV}dx \tag{32}$$

$$\Delta = I_0 \int_0^L (p)dx \tag{33}$$

Eq. (28) can be called as the modified Duffing equation as a result of the Kelvin-Voigt damping term. Eq. (29) represents the linear frequency. Eq. (30) is the nonlinear parameter arising from geometrical nonlinearity. Eq. (31) and Eq. (32) represent damping terms arising from the Kelvin-Voigt model.

The modified Duffing equation can be solved by various perturbation techniques, but in this work, the method of multiple time scales (MTS) [33] will be used. Two time scales are introduced which give rise to:

$$q(t,\epsilon) = q_0(T_0, T_1) + \epsilon q_1(T_0, T_1) + .. \tag{34}$$

where $T_0 = t$ and $T_1 = \epsilon t$. This leads to the transformation of the derivatives of the time scales

$$\frac{d}{dt} = D_0 + \epsilon D_1 \tag{35}$$

$$\frac{d^2}{dt^2} = D_0^2 + 2\epsilon D_0 D_1 + .. \tag{36}$$

This approach assumes small displacements along with small nonlinearity. It also assumes that the nonlinearity, excitation, and damping are all on the same scale ϵ. Hence, with external harmonic excitation, the modified Duffing equation is given by:

$$\ddot{q} + (\beta^2)q + \epsilon(\gamma)q^3 + \epsilon(\delta)q^2\dot{q} + \epsilon(\alpha)\dot{q} = \epsilon F sin(\omega t) \tag{37}$$

Substituting Eq. (35) and (36) into (37) and separating the coefficients of ϵ^0 and ϵ^1 terms;

$$D_0^2 q_0 + \beta^2 q_0 = 0 \tag{38}$$

$$2D_0 D_1 q_0 + D_0^2 q_1 + \beta^2 q_1 + \gamma q_0^3 + D_0 \delta q_0^3 + \alpha q_0 D_0 = F sin(wt) \tag{39}$$

The general solution of Eq. (38) is given by:

$$q_0 = A(T_1)e^{i\beta T_0} + \bar{A}(T_1)e^{-i\beta T_0} \tag{40}$$

Substituting Eq. (40) into (39) and isolating the secular terms ($e^{i\beta T_0}$) which must vanish leads us to:

$$2A'(i\beta) + 3A^2\bar{A} + 3A^2\bar{A}\delta(i\beta) + \alpha A(i\beta) = \frac{F}{2}e^{i\omega T_0} \tag{41}$$

Introducing a detuning parameter "σ" defined as:

$$\omega = \beta + \epsilon\sigma \tag{42}$$

Expressing *A* in polar form and introducing a new parameter φ:

$$\varphi = \sigma T_1 - \Delta \tag{43}$$

$$A = \frac{1}{2}ae^{i\Delta} \tag{44}$$

Substituting Eq. (42-44) into (41) and separating the real and imaginary parts:

$$a' = \frac{1}{2}\mathrm{F}\sin(\varphi) - \frac{3}{8}a^3\delta - \frac{1}{2}\alpha a \tag{45}$$

$$a\varphi' = \frac{1}{2}\mathrm{F}\cos(\varphi) - \frac{3}{8}\frac{a^3}{\beta}\gamma + a\sigma \tag{46}$$

At steady state, the terms *a'* and $a\varphi'$ will vanish. Hence by squaring and adding Eq. (45) and (46), the frequency response equation can be obtained.

$$\left(\frac{3}{8}a^3\delta + \frac{1}{2}\alpha a\right)^2 + \left(a\sigma - \frac{3}{8}\frac{a^3}{\beta}\gamma\right)^2 = \frac{F^2}{4\beta^2} \tag{47}$$

6.1 Theoretical Parameters

It can be noticed from Eq. (24) that the Kelvin-Voigt damping terms represent an equivalent damping for a given laminate sequence. The damping term η in Kelvin-Voigt model can be rewritten in terms of damping ratio by substituting η as:

$$\eta = \zeta\sqrt{\left(C_{11}I_oL^5\Big/I_{yy}\right)} \tag{48}$$

where, ζ is the damping ratio and I_{yy} is the area moment of inertia given by $bh^3/12$.

By substituting Eq. (48) in Eq. (32), equivalent laminate damping which includes the damping characteristics of all lamina can be obtained. The first term on the left hand side of Eq. (47) collectively represents this equivalent damping term. By solving Eq. (47) it can be observed that contribution from δ is minimal compared to the contribution from α. This leads to the observation that Eq. (47) is very similar to the frequency-response equation for the Duffing model as shown by Pasqualini et al. [23] and others.

Since unidirectional laminas are transversely isotropic in nature, their damping characteristics are also transversely isotropic. The on-axis damping matrix is given by:

$$[\zeta_L] = \begin{bmatrix} \zeta_{11} & 0 & 0 \\ 0 & \zeta_{22} & 0 \\ 0 & 0 & \zeta_{66} \end{bmatrix} \tag{49}$$

The off-axis damping matrix for individual lamina can be calculated using:

$$[\zeta_C] = [R]^T [\zeta_L][R^{-1}]^T \tag{50}$$

where, R is the rotation or transformation matrix is given by[34] :

$$[R] = \begin{bmatrix} cos^2\theta & sin^2\theta & -2sin\theta cos\theta \\ sin^2\theta & cos^2\theta & 2sin\theta cos\theta \\ sin\theta cos\theta & -sin\theta cos\theta & cos^2\theta - sin^2\theta \end{bmatrix} \tag{51}$$

The global and local coordinates are related through the angle of the lamina, θ. Using Eq. (50) in Eq. (48) and substituting in Eq. (24) gives the laminate damping which includes the damping characteristic of each lamina. Substituting this into Eq. (32) gives the damping term in the Duffing equation. Similar approach is used to determine the theoretical nonlinearity parameter for different laminate sequences and fiber orientations.

The sequences considered for this study were: [0], [45], [90], [0/90], [90/0], [45/-45] and [0/45/-45/90]. All laminates were 30 layers, 4 mm thick except for the quasi-isotropic which was 48 layers and 6mm thick. The nonlinear parameter and damping ratio were calculated from properties listed in Table 1. The damping matrix given in Eq. (49) has to be determined experimentally, which is beyond the scope of this study. Hence for relative measure, the values given by Youzera et. al. [30] have been used. The nonlinear parameter and damping values calculated from Eq. (30) and (32) for various laminate sequences have been listed in Table 2.

TABLE 1: Material properties of lamina used for numerical and analytical models.

Properties of Laminate	Value
$\mathbf{E_x}$	189 GPa
$\mathbf{E_y}$	6.08 GPa
$\boldsymbol{\nu_{xy}}$	.3
$\mathbf{G_{xy}}$	2.72 GPa
$\boldsymbol{\rho}$	1580 Kg/m^3
$\boldsymbol{\zeta_{11}}$	0.00255
$\boldsymbol{\zeta_{22}}$	0.00425
$\boldsymbol{\zeta_{66}}$	0.0066

6.2 Experiments

The results obtained from NRS testing of unidirectional and MLM were compared with theoretical predictions. Experimental damping ratio was determined for each sequence using the expression:

$$MDR = \frac{f_{hw}}{2f_0} \tag{52}$$

where, f_{hw} is the frequency width at half the peak amplitude of the resonant peak f_0.

Using an approach similar to Pasqualini et al. [23], the nonlinear parameter was extracted from the experimental results using the expression:

$$f_p = \frac{3L^2\gamma_e}{16\pi^3\beta}\varepsilon^2 + \frac{\beta}{2\pi} \tag{53}$$

where, f_p is the nonlinear frequency at peak amplitude, L is the length of the specimen, β is the linear frequency, ε is the strain and γ_e is the experimental nonlinear parameter that is to be determined. It can be observed from Eq. (47) that the nonlinearity parameter and frequency response equation can only describe classical nonlinearity and not the non-classical nonlinearity. Since NCNL materials also exhibit classical nonlinearity at low strain amplitudes as shown in Chapter III, the data in the low strain range, i.e. the classical

zone, was used to determine the classical nonlinear parameter (CNP). The experimental nonlinear parameter extracted for different laminate sequences have been listed in Table 2 along with the experimentally determined damping ratio using Eq. (52).

This experimental CNP represents an equivalent parameter which includes several effects which have not been included in determining the theoretical CNP as mentioned earlier.

6.3 Comparison Between Experiment and Theory

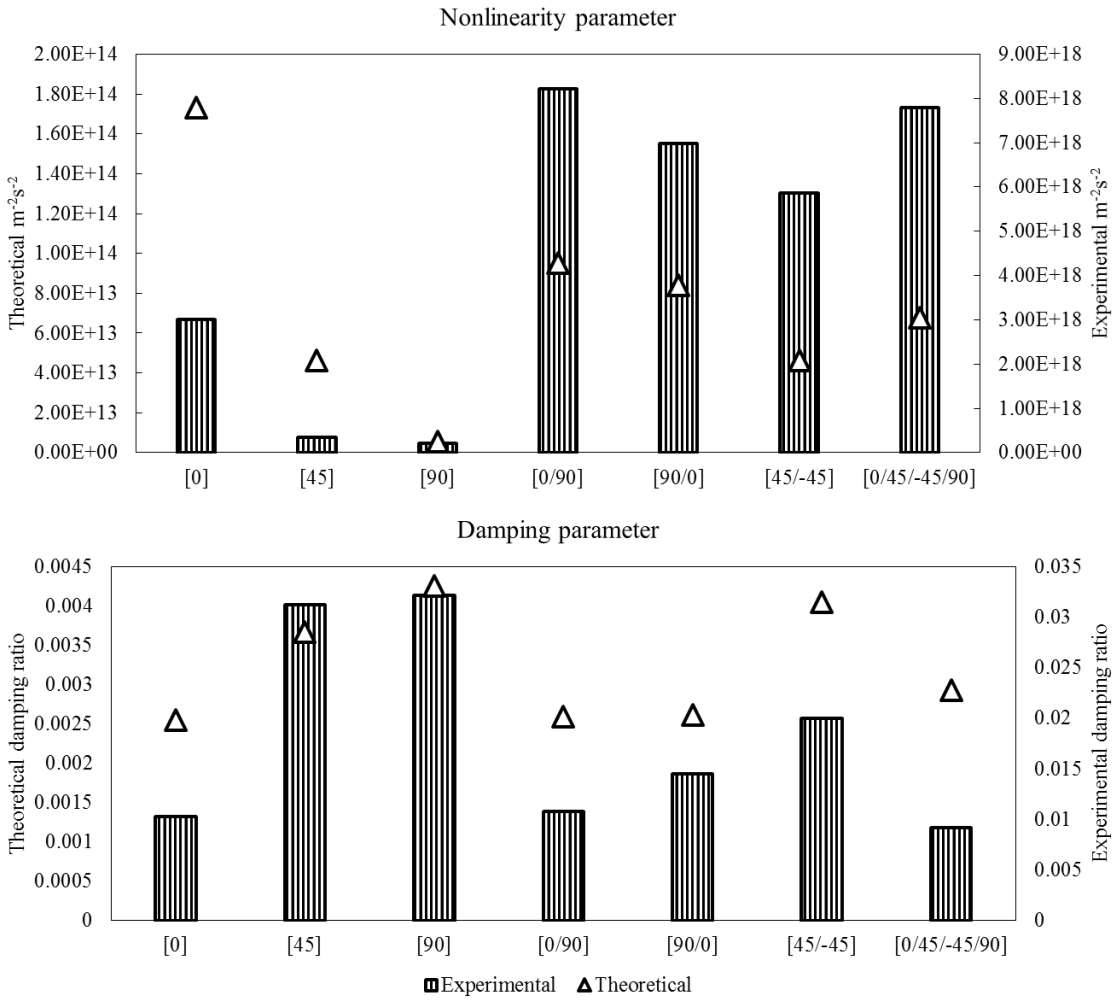

Figure 18: The nonlinearity and damping parameters calculated theoretically and determined experimentally have been plotted together. Although the values between experimental and theoretical are off by factors of 4-5 orders of magnitude, the trend between different laminate sequences is preserved.

The values of CNP and loss factors obtained experimentally and theoretically from Table 2, were plotted together as shown in Figure 18. It can be immediately observed that the theoretical nonlinear parameter values are 4-5 orders of magnitude smaller than the experimentally obtained values. As mentioned earlier the 1D model only considers material geometric nonlinearities and does not consider physical effects such as fiber-matrix interface, inter-lamina effects etc. which can have a much higher contribution to the nonlinear response. From Figure 18, it can be observed that [0] exhibits a higher nonlinear parameter compared to [45] and [90]. MLM laminates have a higher nonlinearity parameter than UD laminates. Comparing the theoretically obtained and experimentally extracted nonlinear parameters, it can be observed that the trend within UD and MLM is preserved in experiment and theory. While experimental nonlinear parameter for [0/90] is higher than [0], the theoretical value of [0/90] is lower than [0]. This difference between experiment and theory can arise from various factors including discounting any inter-lamina effects, and other physical effects as stated earlier. Although quantitatively the values do not match, qualitatively a good correlation can be observed including predicting the response for different laminate sequences.

The damping ratios calculated theoretically and determined experimentally show a much more promising result in terms of the trend in Figure 18. A much closer trend can be obtained by using a different laminate damping model such as the Ni/Adams equation [35]. The current damping model works well in the case of orthotropic laminates where only the diagonal elements exists in Eq. (49). But for a monoclinic case, the entire matrix in Eq. (49) will be filled. Since [45] is monoclinic, the effect of ζ_{16} and ζ_{26} has to be accounted for in the equivalent damping term.

As mentioned earlier, comparing the experimental and analytical nonlinearity parameters would help in identifying the difference between the values due to discounting several factors. The 4-5 orders of magnitude difference experiment and theoretical values may be attributed to some of the physical effects described earlier which were not accounted for in the model.

TABLE 2: Nonlinear parameter and damping ratio calculated theoretically and measured experimentally for different laminate sequences.

Laminate Sequence	**Nonlinear Parameter**		**Damping Ratio**	
	Theoretical	Experimental	Theoretical	Experimental
[0]	-1.73e14	-3.00e18	.00255	0.0103
[45]	-4.62e13	-3.40e17	0.00457	0.03125
[90]	-5.58e12	-2.02e17	0.00425	0.03215
[0/90]	-9.50e13	-8.23e18	0.00259	0.01075
[90/0]	-8.39e13	-6.99e18	0.00261	0.0145
[45/-45]	-4.62e13	-5.87e18	0.00405	0.02
[0/45/-45/90]	-6.78e13	-7.80e18	0.00293	0.0092

Using the theoretical values for nonlinearity parameter and damping ratio from Table 2, Eq. (47) was solved to obtain the resonance curves for increasing levels of excitation as shown in Figure 19(a). As the excitation amplitude increases, the frequency starts decreasing, which is consistent with the experimental observation. The shift in the resonant frequency was calculated by: $\Delta f = f - f_0$ where f is the resonant frequency for a given excitation and f_0 is the resonant frequency at lowest amplitude excitation. Since different laminate sequences have different resonant frequency, the frequency shift was normalized to the lowest amplitude resonant frequency f_0.

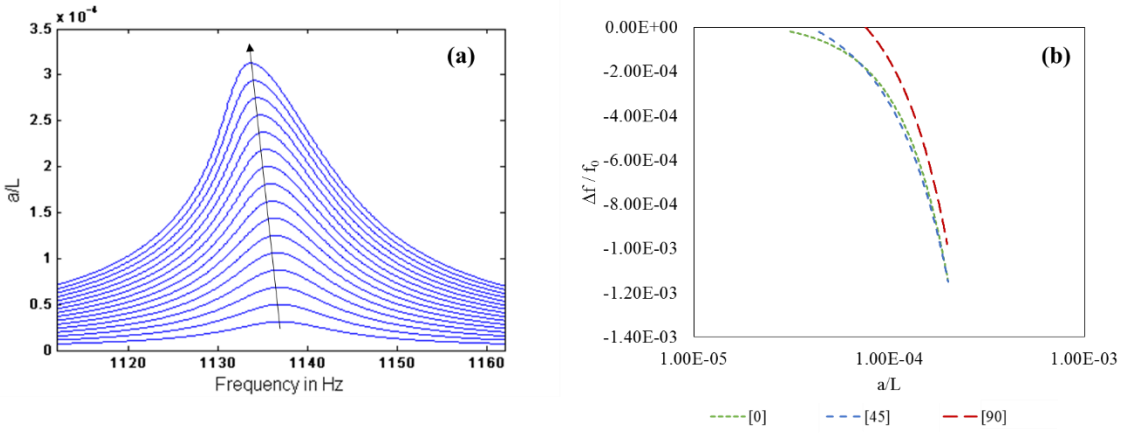

Figure 19: (a) Theoretical resonance curves for various excitation amplitudes simulated from frequency-response equation. (b) The frequency shifts normalized to resonant frequency calculated from the resonance curves from (a) for the three orientation have been plotted against amplitude of vibration normalized to length, "L".

The frequency shift was plotted against *a/L* as shown in Figure 19(b), where *a* is the vibration amplitude normalized to the length of the sample *L*. Significant difference between [0] and [90] can be noticed from the frequency shift plot.

The comparisons between experimental and theoretical frequency shifts cannot be carried out since the value of the nonlinear parameter calculated theoretically is 4-5 orders of magnitude lower than the experimentally determined value. Hence an approach similar to Pasqualini et al. was used by extracting the parameter values from experiment in the classical zone using the model equations, i.e. Eq. (52) and Eq. (53). These were used in the frequency-response equation given by Eq. (47) to generate the semi-analytical experimental resonance curve. The data obtained using this technique would help in verifying if the nonlinear model presented here is able to capture the physical phenomenon as observed in the experiments in the classical zone. For the comparison, only data from [0], [45] and [90] have been considered.

The experimental and model predicted frequency shifts for different laminate sequences have been plotted in Figure 20(a), (b) and (c). From Figure 20(a), it can be observed that the analytical data for [0] does not match very well with the experimentally obtained data. This can be due to lack of measurement sensitivities at very low amplitudes coupled with other nonlinear contributions from sources not considered in this work as described in Chapter III. But a better fit for [45] can be observed from Figure 20(b). Similarly [90] exhibits a good agreement between experiment and the model prediction as can be seen in Figure 20(c).

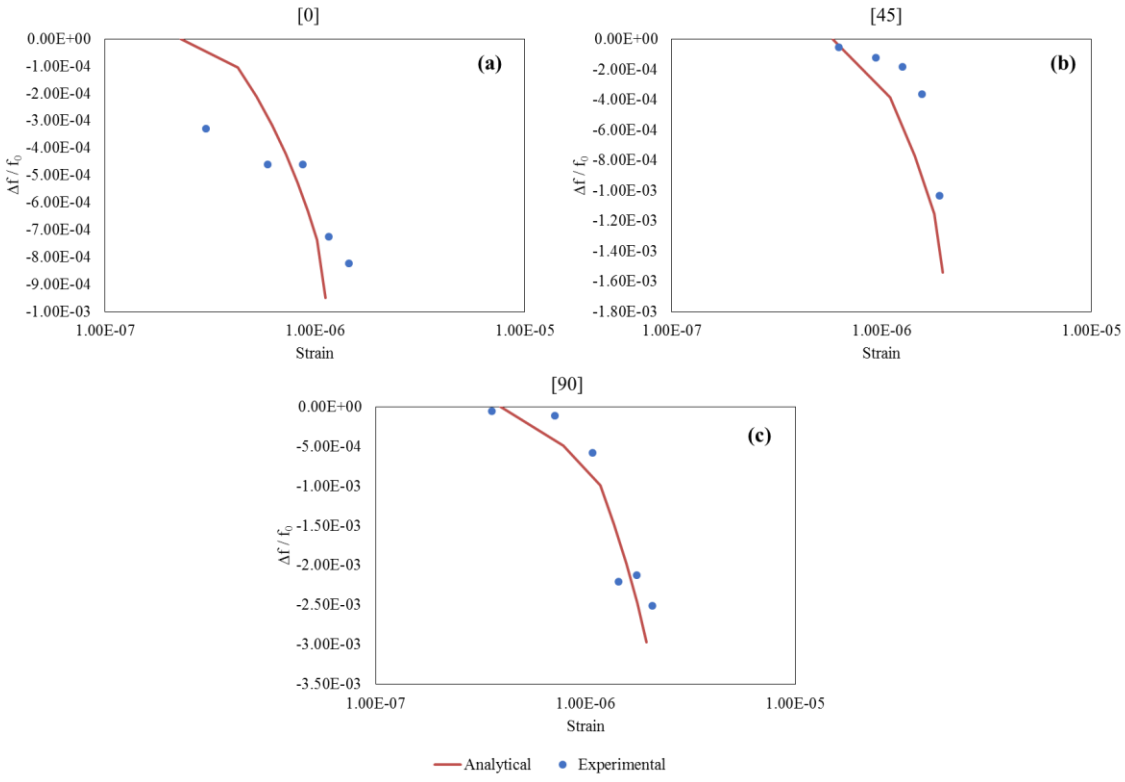

Figure 20: The frequency shift observed experimentally compared to the theoretical predictions from frequency-response equation for: (a) 0^0 laminate, (b) 45^0 laminate, (c) 90^0 laminate. The solid line represents the analytical solution and points represent the experimental data.

Several researchers [20, 36-38] have tried to create nonlinear models which captures the non-classical nonlinear nature of certain materials. But most of them are phenomenological models, not physical models. In an effort to develop such a model, the current study used a viscoelastic formulation to capture the non-classical nature. Using geometric nonlinearity and linear viscoelasticity, the modified Duffing equation was obtained. It is well known that three parameters namely damping, linear frequency, and nonlinearity parameter control the frequency response equation. The viscoelastic term in the Kelvin-Voigt model does not contribute to nonlinearity, rather the contribution comes directly in the form of stiffness.

The importance of this work lies in the ability of the model to capture the physical effect that was observed experimentally. Although pure theoretical CNP values cannot be directly compared to experiment, qualitatively a good agreement can be observed. Furthermore, by substituting the experimental CNP values into the model equation, a good agreement between experimental data and model predictions was observed.

The geometric nonlinearity considered in this work can only simulate the classic nonlinear zone as can be seen in Figure 20. The 3rd strain zone with non-classical nonlinearity exhibiting linear frequency shifts was not observed using the model used in this study. This suggests that using a linear stress-strain relationship with linear Kelvin-Voigt damping term will not simulate the non-classical nonlinear nature of the composites and will only simulate the classical nonlinearity. A nonlinear Kelvin-Voigt damping model will be reserved for future work. Similarly a nonlinear stress-strain relationship coupled with nonlinear strain-displacement relationship will be explored as a part of future work.

CHAPTER VII

DISCUSSION AND CONCLUSION

7.1 Discussions

To observer the influence of fiber type on CNP, the nonlinear parameter for continuous and woven fabric from Table 3 was plotted into a column plot as shown in Figure 21. Only experimental values for woven laminate could be obtained since theoretically calculating the nonlinear parameter from woven fabric is beyond the scope of this work. The WCP has a lower nonlinear value compared to the [0/90]C, while [45/-45]W exhibits a higher nonlinear value compared to [45/-45]C. To interpret and explain this trend would require a physical model considering contributions from many nonlinear sources.

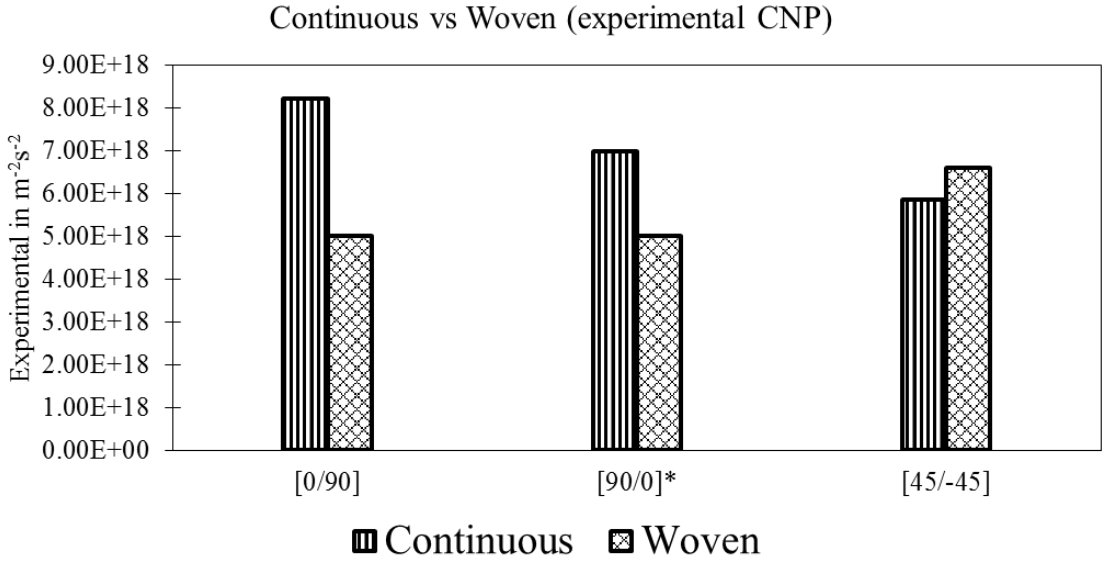

Figure 21: A comparison of the experimental nonlinearity parameter extracted from Eq. (51) between continuous and woven fabric. A higher level of nonlinearity can be observed for the continuous compared to woven for [0/90], whereas the [45/-45]W shows slightly higher nonlinearity than the continuous fabric.

TABLE 3: Nonlinear parameters extracted from experiment comparing continuous and woven fabric.

Laminate Sequence	Continuous fabric	Woven fabric
[0/90]	-8.225e18	-5.004e18 (WCP)
[90/0]	-6.98e18	-5.004e18 (WCP)
[45/-45]	-5.867e18	-6.605e18

For material characterization and NDE of composites, both the classical nonlinear and non-classical nonlinear parameters are important. The non-classical nonlinear parameter can be calculated as shown by Van Den Abelee [10]:

$$C_1 = \frac{(f_0 - f)/f_0}{\Delta\epsilon} \tag{54}$$

where, f is the resonance frequency at strain amplitude $\Delta\varepsilon$, and f_0 is the low amplitude resonance frequency. The non-classical parameter C_1 calculated from Eq. (54) was compared between different laminate sequences as shown in Figure 22.

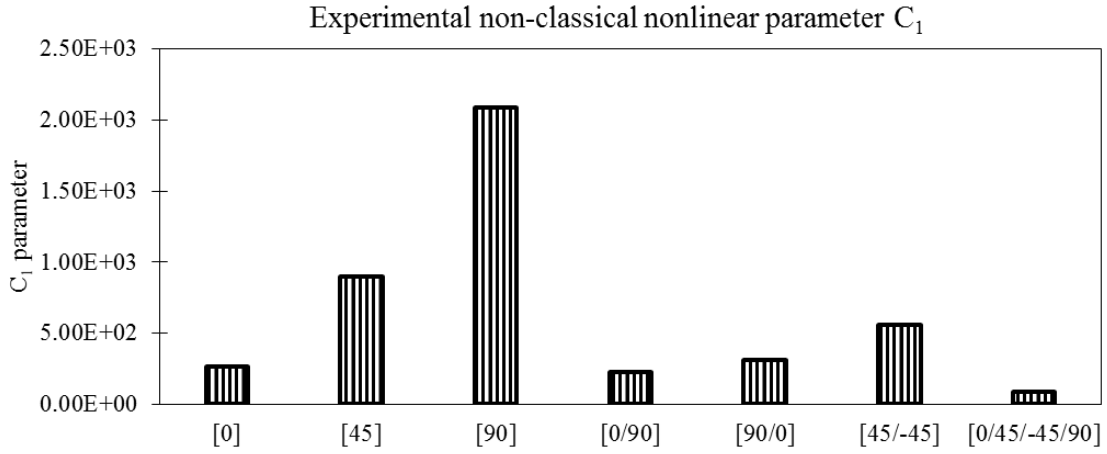

Figure 22: The experimental non-classical nonlinearity parameter C_1 calculated from Eq. (54) for different laminate sequences have been compared.

Consistent with the results observed earlier in Chapter 2 & 3, 90^0 exhibits highest C_1 values compared to 0^0, 45^0 and MLM. With decrease in anisotropy, the C_1 values for MLM reduces below the value for 0^0 with QIS exhibiting the lowest C_1 value. The C_1 values for continuous and woven fabric was compared in Figure 23. The WCP laminate has lower C_1 value compared to [0/90]C and [90/0]C, while the [45/-45]W is slightly lower than [45/-45]C.

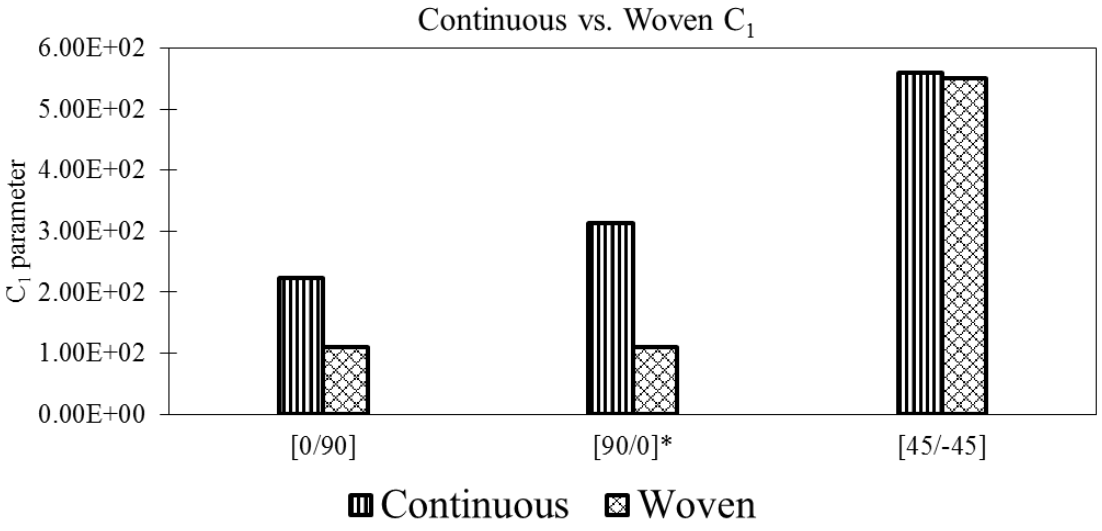

Figure 23: The experimental non-classical nonlinearity parameter C_1 calculated from Eq. (54) for continuous and woven fabrics have been compared.

The knowledge of C_1 parameter is vital for NDE of composite laminates using NEWS techniques. The large difference in baseline C_1 value between 90^0 and QIS highlights the need for a thorough baseline study for the given laminate orientation, since a large baseline nonlinear response can easily be mistaken for damaged state.

Mode selection can also alter the results significantly, i.e. results can vary between a flexural mode and a torsional mode. In the current study only the fundamental flexural

mode was used to perform the NRS tests. To understand the influence of the chosen mode, a linear finite element modal analysis was performed on 0^0 laminate to find the higher order shear or torsional mode. NRS experiments were repeated for the torsional mode and the results are shown in Figure 24. The fundamental bending mode was observed at 974 Hz while the torsional mode could be observed at 4345 Hz. The bending mode shows a much smaller frequency shift compared to the torsional mode even at lower velocity as seen Figure 24. The properties along the length of the sample will influence the flexural mode, whereas the shear properties will influence the torsional mode. The higher NCNL response from a shear mode, suggests that shear or sliding action has a bigger role to play in the contributions towards NCNL behavior.

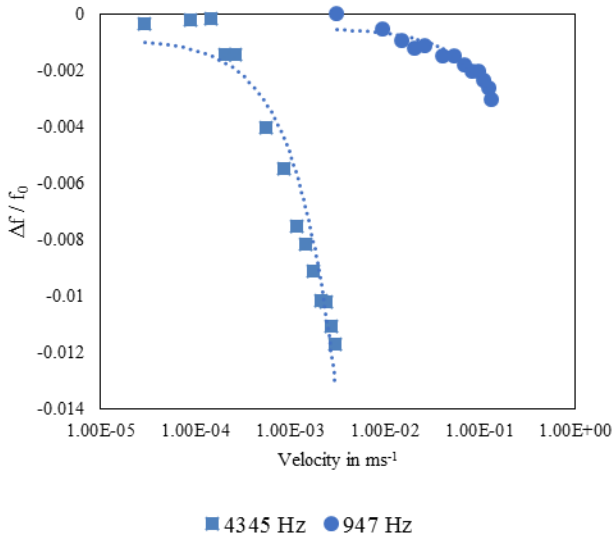

Figure 24: Influence of mode on inherent nonlinearity. Mode at 947 Hz is the first order bending mode, while mode at 4345 Hz is a shear or torsional mode. The torsional mode exhibits much higher nonlinearities at lower excitation velocities compared to the bending mode.

7.2 Summary and Conclusion

The current work focused on investigating the influence of fiber orientation on inherent acoustic nonlinearity of composites. The initial hypothesis was that fiber reinforced composites which can be multi-material, multi-layered structures may act like rock and other geomaterials in terms of nonlinear response, i.e. non-classical nonlinear in nature. NRS tests were performed by collecting resonant frequency sweeps for increasing excitation voltages. Based on the frequency shifts in the various strain zones, the responses were found to be similar to that of NCNL materials. It was observed that 90^0 had the highest shift in frequency, followed by 45^0 and 0^0. A linear increase in MDR was observed with 90^0 increasing the highest followed by 45^0 and 0^0 consistent with the frequency shift. Similarly the 3rd harmonic scaled quadratic as a function of the fundamental. These results show that composites demonstrate a NCNL nature and reveal how the fiber orientation can affect the non-classical nonlinear response of composites.

NRS tests were carried out on rectangular coupons fabricated with different laminate sequences; [0/90], [90/0], [45/-45], [0,45/-45/90] and different fabric type; continuous and woven fabric. The observed nonlinear response was compared to nonlinear response from continuous UD fabric which showed that MLM reduces the non-classical nonlinear contribution.

To explore the source of nonlinearity, a nonlinear viscoelastic model based on geometric nonlinearity and Kelvin-Voigt damping term was developed. A forced vibration analysis was performed which resulted in solving the modified Duffing equation to obtain the frequency-response equation. Good agreement in trend was observed between the theoretically obtained nonlinear parameter and damping values. This is a very simple first

order model with no shear or rotational effects, but a higher order model using third or fourth order shear deformation theory might be able to match the results and trend better. The experimental results obtained for woven fabric was compared to continuous fabric which showed that classical nonlinearity is lower in woven composite compared to continuous fabric composites. Theoretical resonance curves show that a quadratic shift in frequency can be captured using the model. A semi-analytical experiment model was compared with the experimentally obtained results, which showed a nominally good agreement. Modeling and understanding the nonlinear response of composites is important due to the fact that composites are anisotropic and cannot be generalized. Each laminate sequence exhibits a certain level of nonlinearity different from other sequences, and hence generalization of nonlinearity is not possible. Modeling the nonlinearity based on laminate sequence will help in characterizing the baseline response of composites before applying any type of nondestructive evaluation tool for inspection of flaws or defects.

Furthermore, the non-classical nonlinear parameter was also determined for all laminates. It was observed that the laminates which exhibited highest classical nonlinearity, exhibited least non-classical nonlinearity and vice-versa. This suggests that a classical nonlinear strain zone exists which is described by the classical nonlinear parameter and a non-classical strain zone with hysteresis, conditioning etc. exists which dominates over classical nonlinearity. Woven fabric exhibited lower non-classical nonlinearity compared to continuous fabric. Explaining these trends require physical models with the ability to capture small nonlinear sources like crazing, fiber-fiber interaction, inter-lamina effects etc.

The importance of the study lies in characterizing the baseline nonlinear response of composites, which is very vital for any nonlinear NDE of composites. By studying the effect of fiber orientation, laminate sequence and fabric type, the baseline study can be extended for any combinations of these making it easier to characterize and inspect composite structures. The model will help in determining the baseline nonlinearity of a certain laminate sequence before any NDE has to be performed which, will help to quantify the baseline nonlinearity better.

REFERENCES

[1] I. G. Scott, C. M. Scala, “A review of non-destructive testing of composite materials”, NDT International, Vol 15, Issue 2, April 1982, pp: 75-86

[2] J. Summerscales (Ed), “Non-destructive testing of fiber-reinforced plastics composites”, Vol. 1, 1987, London, Elsevier Applied Science, pp: 1-278.

[3] W. Sachse, B. Castagnede, I. Grabec, K. Y. Kim, R. L. Weaver, “Recent developments in quantitative ultrasonic NDE of composites”, Ultrasonics, Vol. 28, Issue 2, March 1990, pp: 97-104.

[4] R. D. Adams, P. Cawley, “A review of defect types and nondestructive testing techniques for composites and bonded joints”, Vol. 21, Issue 4, August 1988, pp: 208-222.

[5] Y. Bar-Cohen, “Ultrasonic NDE of composites – A review”, Solid Mechanics research for quantitative non-destructive evaluation, Springer Netherlands, 1987, pp: 187-201.

[6] D. E. Chimenti, R. W. Martin, “Nondestructive evaluation of composite laminates by leaky Lamb waves”, Ultrasonics, Vol. 29, Issue 1, January 1991, pp: 13-21.

[7] N. Guo, P. Cawley, “The interaction of Lamb waves with delaminations in composite laminates”, J. Acoust. Soc. Am. 94, pp: 2240-2246 (1993).

[8] V. Dayal and V. K. Kinra, "Leaky Lamb Waves in an Anisotropic Plate II - NDE of Matrix Cracks in Fiber-Reinforced Composites," *J. Acoustical Society of America*, 89(4) Pt.1, pp: 1590-1598, 1991.

[9] R. A. Guyer, P. A. Johnson, “Nonlinear mesoscopic elasticity: Evidence for a new class of materials” Physics Today, April 1999, pp: 30-36.

[10] K. E-A. Van Den Abeele, A. Sutin, J. Carmeliet, P. A. Johnson, "Micro-damage diagnostics using nonlinear elastic wave spectroscopy (NEWS)" NDT&E International, 34(2001), pp 239-248.

[11] K. E-A. Van Den Abeele, P. A. Johnson, A. Sutin, "Nonlinear elastic wave spectroscopy (NEWS) techniques to discern material damage, Part I: Nonlinear wave modulation spectroscopy (NWMS)" Res Nondestr Eval, 12(2000) pp: 17-30.

[12] K. E-A. Van Den Abeele, J. Carmeliet, J. A. Ten Cate, P. A. Johnson, "Nonlinear elastic wave spectroscopy (NEWS) techniques to discern material damage, Part II: Single-mode nonlinear resonance acoustic spectroscopy" Res Nondestr Eval, 12 (2000) pp: 31-42.

[13] I. Solodov, J. Wackerl, K. Pfleiderer, G. Busse, "Nonlinear self-modulation and subharmonic acoustic spectroscopy for damage detection and location", Appl. Phys. Lett., 84 (2004), pp: 5386-5388.

[14] M. Meo, U. Polimeno, G. Zumpano, "Detecting damage in composite materials using nonlinear elastic wave spectroscopy methods", Appl Compos Mater, 15 (2008) pp: 115-126.

[15] M. Meo, G. Zumpano, "Nonlinear elastic wave spectroscopy identification of impact damage on a sandwich plate", Composite structures 71 (2005) pp: 469-474.

[16] K. E-A. Van Den Abeele, P. Y Le Bas, B. Van Damme, T. Katkowski, "Quantification of material nonlinearity in relation to microdamage density using nonlinear reverberation spectroscopy: Experimental and theoretical study" J. Acoust. Soc. AM. 126 (3) Sep 2009 pp: 963-972.

[17] F. Aymerich, W. J. Stasewski, "Impact damage detection in composite laminates using nonlinear acoustics", Composites: Part A, 41 (2010) pp: 1084-1092.

[18] A. Novak, M. Bentahar, V. Tournat, R. El Guerjouma, L. Simon, "Nonlinear acoustic characterization of micro-damaged materials through higher harmonic resonance analysis", NDT & E International, 45(1), pp: 1-8.

[19] Y. Baccouche, M. Bentahar, C. Mechri, R. El Guerjouma, M. H. B. Ghozlen "Hysteretic nonlinearity analysis in damaged composite plates using guided waves" J. Acoust. Soc. Am. 133 (4), EL256 April 2013.

[20] K. E-A. Van Den Abeele, P. A. Johnson, R. A. Guyer, K. R. McCall, "On the quasi-analytic treatment of hysteretic nonlinear response in elastic wave propagation" J. Acoust. Soc. Am. 101 (4) April 1997, pp: 1885-1898.

[21] P. A. Johnson, B Zinszner, P. N. J. Rasolofosaon, "Resonance and elastic nonlinear phenomena in rock", J. Geophysical Research. Vol. 101, No. B5, May 1996, pp: 11553-11564.

[22] R. A. Guyer, J. Tencate, P. Johnson, "Hysteresis and the dynamic elasticity of consolidated granular materials", Physical Rev. Letters, Vol. 82(16), April 1999, pp: 3280-3283.

[23] D. Pasqualini, K. Heitmann, J. A. TenCate, S. Habib, D. Higdon, P. A. Johnson, "Noneqilibrium and nonlinear dynamics in Berea and Fontainebleau sandstones: Low-strain regime" J. Geophys. Res. Vol. 112, B01204 (2007).

[24] L. Landau and E. Lifshitz, *Theory of Elasticity, Vol. 7, Course of Theoretical Physics*, 3rd ed. (Butterworth-Heinemann,Waltham, MA, 1986), pp. 1–195.

[25] J. W. Strutt (Lord Rayleigh), "The Theory of Sound", Vol 1, Chap. 8, New York, Dover, 1877.

[26] L. Azrar, R. Benamar, R. G. White, "A semi-analytical approach to the non-linear dynamic response problem of S-S and C-C beams at large vibration amplitudes Part1: General theory and application to the single mode approach to free and forced vibration analysis" J. Sound and Vibration, 224(2), 1999, pp: 183-207.

[27] L. Azrar, R. Benamar, R. G. White, "A semi-analytical approach to the non-linear dynamic response problem of beams at large vibration amplitudes, Part II: Multimode approach to the steady state forced periodic response", J. Sound and Vibration, 255(1), 2002, pp: 1-41.

[28] S. N. Mahmoodi, S. E. Khadem, N. Jalili, "Theoretical development and closed-form solution of nonlinear vibrations of a directly excited nanotube-reinforced composite cantilevered beam", Arch. Appl. Mech (2006), 75, pp: 153-163.

[29] S. N. Mahmoodi, N. Jalili, S. E. Khadem, "An experimental investigation of nonlinear vibration and frequency response analysis of cantilever viscoelastic beams", J. Sound and Vibration, 311 (2008), pp: 1409-1419.

[30] H. Youzera, S. A. Meftah, N. Challamel, A. Tounsi, "Nonlinear damping and forced vibration analysis of laminated composite beams", Composites: Part B, 43 (2012) pp: 1147-1154.

[31] A. Shooshtari, M. Rafiee, "Nonlinear forced vibration analysis of clamped functionally graded beams", Acta. Mech. 221 (2011), pp: 23-38.

[32] Reddy, J. N. (2004). "Mechanics of laminated composite plates and shells: theory and analysis", Chapter 3, 2nd ed. CRC press, (Boca Raton, Florida), 2004.

[33] A. H. Nayfeh, D. T. Mook, "Nonlinear Oscillations", Wiley, New York (1979).

[34] A. K. Kaw, "Mechanics of composite materials", CRC press, Boca Raton, Florida, 1997.

[35] R. G. Ni, R. D. Adams, "The damping and dynamic moduli of symmetric laminated composite beams- Theoretical and experimental results", J. Compos. Mater. 18(2), 1984, pp: 104-21.

[36] P. P. Delsanto, M. Scalerandi, "Modeling nonclassical nonlinearity, conditioning and slow dynamics effects in mesoscopic elastic materials", Physical Rev. B. Vol. 68 (2003), 064107.

[37] K. R. McCall, R. A. Guyer, "Equation of state and wave propagation in hysteretic nonlinear elastic materials", J. Goephys. Research. Vol. 99, No. B12, (1994) pp: 23887-23897.

[38] K. E-A. Van Den Abeele, “Elastic pulsed wave propagation in media with second- or higher-order nonlinearity. Part I. Theoretical framework”, J. Acoust. Soc. Am. 99(6) June 1996, pp: 3334-3345.

[39] W-C. Wu, W. H. Prosser, “Harmonic generation measurements in unidirectional graphite/epoxy composites”, Review of progress in Qualitative Nondestructive Evaluation, Vol. 10. B, Edited by D. O. Thompson and D. E. Chimenti, Plenum Press, New York, 1991. pp: 1477- 1482.

APPENDIX

NONLINEAR MODEL II

This section presents a work in progress for modeling nonlinear response of laminate beam where the source of nonlinearity is the stress-strain relationship instead of geometric nonlinearity as shown in this work.

A nonlinear stress-strain relationship was described as:

$$\sigma_{ij} = C_{ijkl}\varepsilon_{kl} + C_{ijklmn}\varepsilon_{kl}\varepsilon_{mn} \tag{55}$$

where, C_{ijkl} represents the seconds order elastic constants, and C_{ijklmn} represents the third order elastic constants. For an orthotropic material, there are 9 second order elastic constants and 20 third order constants. Using Voigt notation, C_{ijkl} and C_{ijkl} can be rewritten as C_{ij} and C_{ijk}. Since this is 1D case, only C_{111} and C_{11} will influence the results.

A linear strain-displacement relationship was chosen to discount for any geometric nonlinearities.

$$\varepsilon_{xx} = \frac{\partial u_0}{\partial x} - z\frac{\partial^2 w_0}{\partial x^2} \tag{56}$$

Using a similar approach to Chapter 4, the force and moment resultants can be written as:

$$N_{xx} = A_{11}(u_0') - B_{11}w_0'' + A_{111}(u_0')^2 + D_{111}(w_0'')^2 - 2B_{111}u_0'w_0'' \tag{57}$$

$$M_{xx} = B_{11}(u_0') - D_{11}w_0'' + B_{111}(u_0')^2 + E_{111}(w_0'')^2 - 2D_{111}u_0'w_0'' \tag{58}$$

where,

$$(A_{11}, B_{11}, D_{11}) = \int_{-h/2}^{h/2} C_{11}(1, z, z^2)dz \tag{59}$$

$$(A_{111}, B_{111}, D_{111}, E_{111}) = \int_{-h/2}^{h/2} C_{111}(1, z, z^2, z^3)dz \tag{60}$$

Using boundary conditions, Eq. (57) can be writing in terms of the transverse displacements alone. Further, substituting Eq. (57) and Eq. (58) into the equation of motion, Eq. (16), and expressing the transverse displacement as *W(x,t) = q(t) p(x)*, the modified undamped Duffing equation can be obtained.

$$\ddot{q} + (\omega^2)q + (\Gamma)q^3 + (\Psi)q^2 = F \tag{61}$$

where,

$$\omega^2 = \frac{D_{11}}{\Delta}\int_0^L p^{IV}dx \tag{62}$$

$$\Gamma = -\frac{D_{111}}{\Delta}\int_0^L (p'')^3 dx \tag{63}$$

$$\Psi = \frac{E_{111}}{\Delta}\left(\int_0^L p''p^{IV}dx + \int_0^L p'''dx\right) \tag{64}$$

$$\Delta = I_0 \int_0^L (m)dx \tag{65}$$

Eq. (61) is the modified Duffing equation as a result of nonlinear stress strain relationship. Eq. (62) represents the linear frequency, Eq. (63) is the nonlinear parameter arising from third order elastic constants.

Eq. (61) can be solved using perturbation technique as shown earlier to obtain the solution:

$$\left(a\sigma - \frac{3}{8}\frac{a^3}{\omega}\Gamma\right)^2 = \frac{F^2}{4\omega^2} \tag{66}$$

This solution is similar to the solution of the undamped Duffing equation, with the nonlinearity source being the third order elastic constants. Nonlinearity controlled by the third order elastic constants would lead one to believe that the gap between experimental and theoretical nonlinearity parameter would be brought closer at least by an order of magnitude, but on the contrary the value of Γ for [0] is much smaller than γ, i.e. 9.6e8, compared to 1.73e14 from geometric nonlinearities. The third order constant used to calculate Γ was taken from Wu et. al.[39] as -829 GPa. Although this model suggests that geometric nonlinearities can contribute to a higher nonlinear response, a combined model with geometric nonlinearity and material nonlinearity might be able explain part of the phenomenon. This will be reserved for future work.